3. Results and Discussions

3.1 Crack Growth Tests on Nonirradiated Stainless Steel Weld HAZ Specimens

This section presents the results of crack growth tests in the BWR environment with nonirradiated specimens of Type 304L GG core shroud H5 weld HAZ and Type 304 laboratory–prepared weld HAZ. The GG weld HAZ specimens were from the bottom shell of the H5 weld and were in the as–welded (GG5B–A) and as–welded plus thermally treated condition (GG3B–A–TT). The Type 304 SS laboratory–prepared weld HAZ specimen was in the as–welded plus thermally treated condition (853B–A–TT).

3.1.1 Specimen GG5B–A of the HAZ from Grand Gulf Core Shroud H5 SA Weld, Test CGR-10

The environmental and loading conditions, experimental CGRs, allowed values of K_{max} from the K/size criterion in Eq. 13, and the deviation of applied K_{max} from the allowed value are given in Table 3 for Specimen GG5B–A. During most test periods, K_{max} was maintained approximately constant by periodic load shedding. The test was started in high–DO water (≈580 ppb DO in effluent) and a flow rate of 140 mL/min. Because of a faulty reference electrode, the ECPs of the Pt and SS electrodes in the effluent could not be monitored during the test. The water conductivity was monitored continuously.

Precracking was initiated at R = 0.23, K_{max} ≈15 MPa $m^{1/2}$, and a triangular waveform. After ≈0.6 mm advance, R was increased incrementally to 0.7 and the waveform changed to a slow/fast sawtooth with a rise time of 30 s; in all cases the fast rate (time to unload) was 2 s. The changes in the crack length and K_{max} with time during the various test periods are shown in Figs. 14a–c. During the initial 300–h test period (precracking and test periods 1–2b in Table 3), no environmental enhancement was observed in the measured growth rates. Also, decreasing the flow rate from 140 to 35 mL/min had little or no effect on the CGRs, although the conductivity increased from ≈0.07 to 0.14 µS/cm.

Table 3. Crack growth results for Specimen GG5B–A[a] of Type 304L HAZ in high–purity water at 289°C.

Test Period[b]	Test Time, h	Flow Rate, CC/min	Cond.,[c] µS/cm	O_2 Conc.,[c] ppb	R Load Ratio	Rise Time, s	Down Time, s	Hold Time, s	K_{max}, MPa·$m^{1/2}$	ΔK, MPa·$m^{1/2}$	Growth Rate, m/s	Allowed K_{max},[d] MPa·$m^{1/2}$	Deviation in K_{max},[d] %
Pre a	97	140	0.07	580	0.23	0.25	0.25	0	16.7	12.9	7.57E-08	19.3	-13
Pre b	98	140	0.07	580	0.23	0.25	0.25	0	15.0	11.5	3.42E-08	19.1	-22
Pre c	114	140	0.08	590	0.23	7.5	7.5	0	14.2	11.0	3.59E-10	19.1	-25
Pre d	120	140	0.07	590	0.23	0.50	0.50	0	15.7	12.1	3.40E-08	18.7	-16
1	143	140	0.08	485	0.52	30	2	0	15.5	7.4	5.85E-11	18.6	-17
2a	259	30	0.12	440	0.71	30	2	0	17.0	4.9	negligible	18.6	-9
2b	306	35	0.14	450	0.71	30	2	0	17.0	4.9	1.52E-11	18.6	-9
2c*	337	35	0.14	464	0.72	30	2	0	20.6	5.8	3.15E-10	18.6	11
3*	407	35	0.14	460	0.71	300	2	0	20.8	6.0	1.81E-10	18.5	13
4*	455	35	0.13	500	0.71	1,000	2	0	20.9	6.1	1.26E-10	18.5	13
5	572	35	0.13	500	0.71	12	12	3600	21.1	–	6.01E-11	18.4	14
6	646	105	0.08	500	0.71	12	12	3600	26.5	–	1.72E-10	18.3	45
7	692	105	0.07	500	0.71	12	12	3600	26.9	–	1.55E-10	18.2	47
8	767	105	0.07	500	0.71	1,000	2	0	27.4	7.9	3.18E-10	18.1	51

[a]Nonirradiated Grand Gulf H5 SA weld bottom shell HAZ, as–welded condition.
[b]An asterisk indicates environmental enhancement of growth rates under cyclic loading.
[c]Represents values in the effluent.
[d]Based on flow stress.

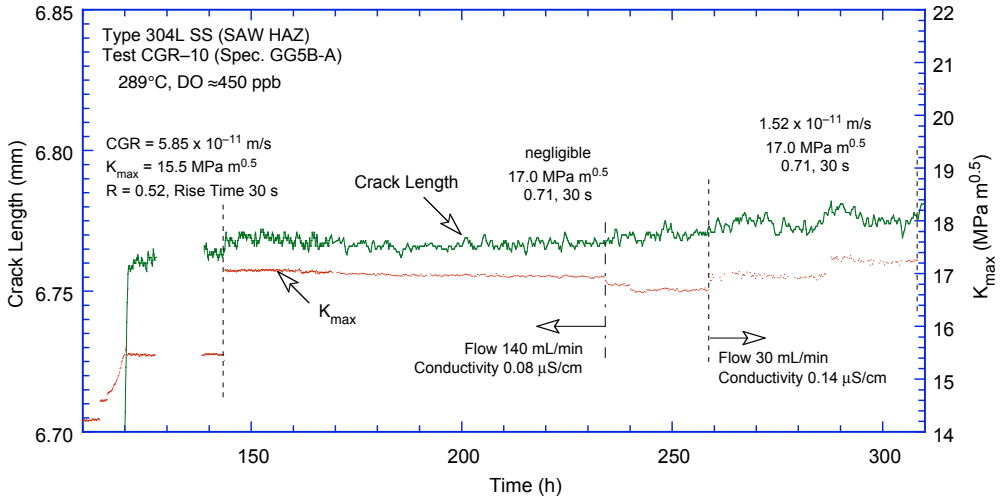

(a)

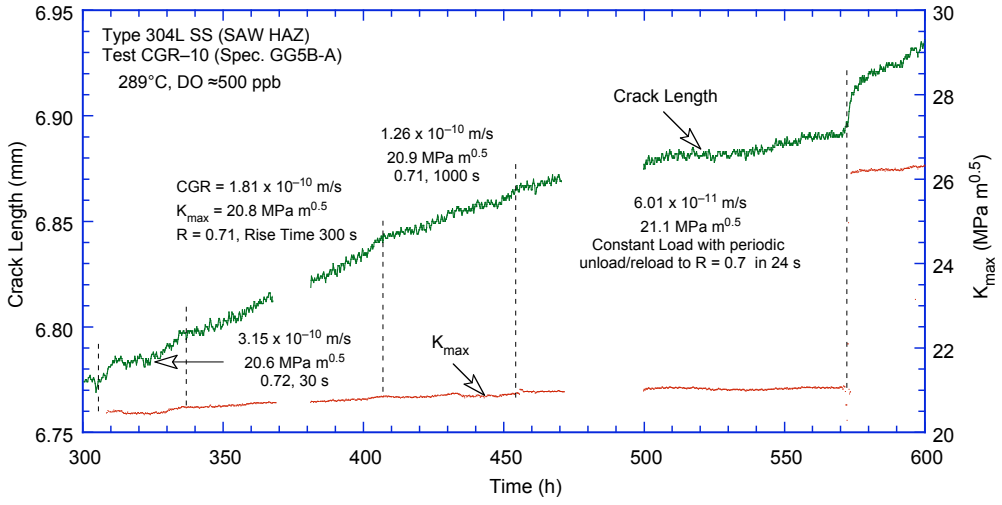

(b)

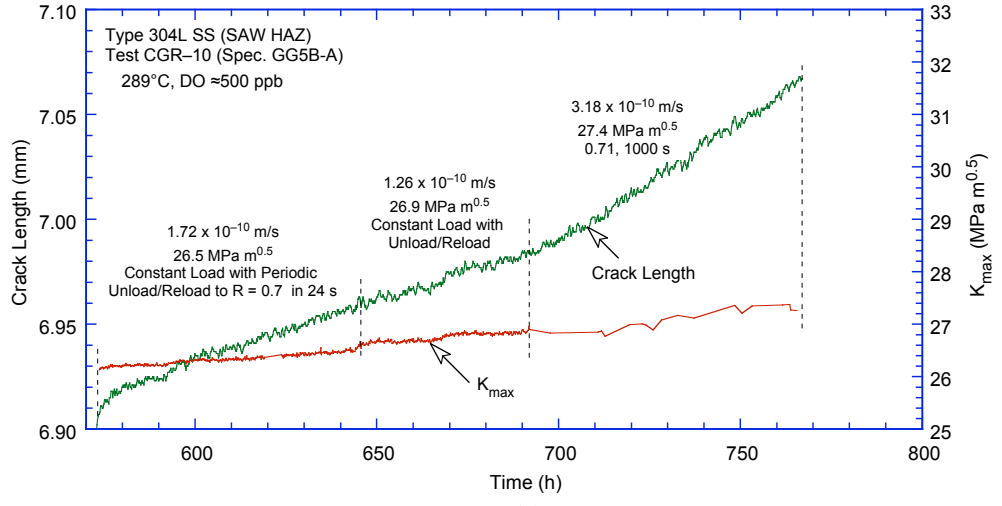

(c)

Figure 14. Crack–length–vs.–time plots for nonirradiated Type 304L bottom shell HAZ from the Grand Gulf H5 SA weld in high–purity water at 289°C during test periods (a) precracking–3, (b) 4-6, and (c) 7–8.

After ≈310 h, K_{max} was increased to ≈20 MPa $m^{1/2}$, and rise time increased to 300 s and then 1000 s. Under these conditions, environmental enhancement of CGRs is observed. After ≈450 h the loading waveform was changed to a trapezoidal shape with 3600–s hold period and 12–s unload and reload periods. For Specimen GG5B–A, the experimental K_{max} values were generally higher (≈13% higher during test periods 2c–5 and ≈45–50% higher during periods 6–8) than the allowed K_{max} based on flow stress and Eq. 13.

Photomicrographs of the fracture surface of the two halves of the broken specimen are shown in Fig. 15. A relatively straight crack front is observed. The crack lengths were measured by both optical and scanning electron microscopy. The results showed very good agreement with the values estimated from the DC potential measurements; the difference in measured and estimated values was <5%.

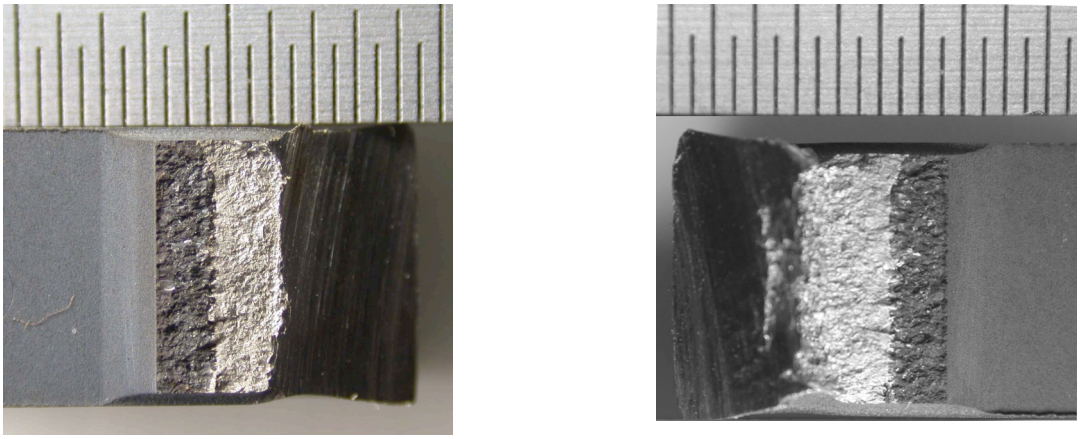

(a) (b)

Figure 15. Photomicrograph of the fracture surface of Specimen GG5B–A.

After the test both halves of the fractured specimen were cleaned chemically to remove the surface oxide film using the procedure described in Section 2.2.2, and the fracture surface was examined by SEM. A micrograph of the fracture surface for Specimen GG5B–A is shown in Fig 16. Micrographs showing a slice of the entire crack advance during the CGR test and typical fracture morphology at select locations on the surface are shown in Fig. 17a–d. A predominantly transgranular (TG) fracture morphology is observed for the entire test. Most of the TG facets show a well–defined river pattern (Fig 17a). Also, a TG fracture with the river pattern is also observed from room–temperature cycling after the test (Fig. 17d) to mark the final crack front.

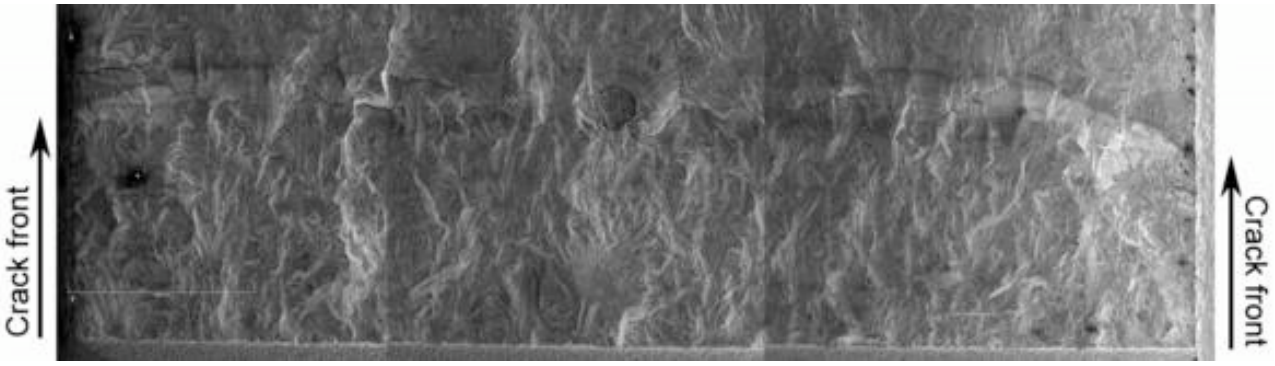

Figure 16. Micrograph of the fracture surface of Specimen GG5B–A tested in high–DO water at 289°C.

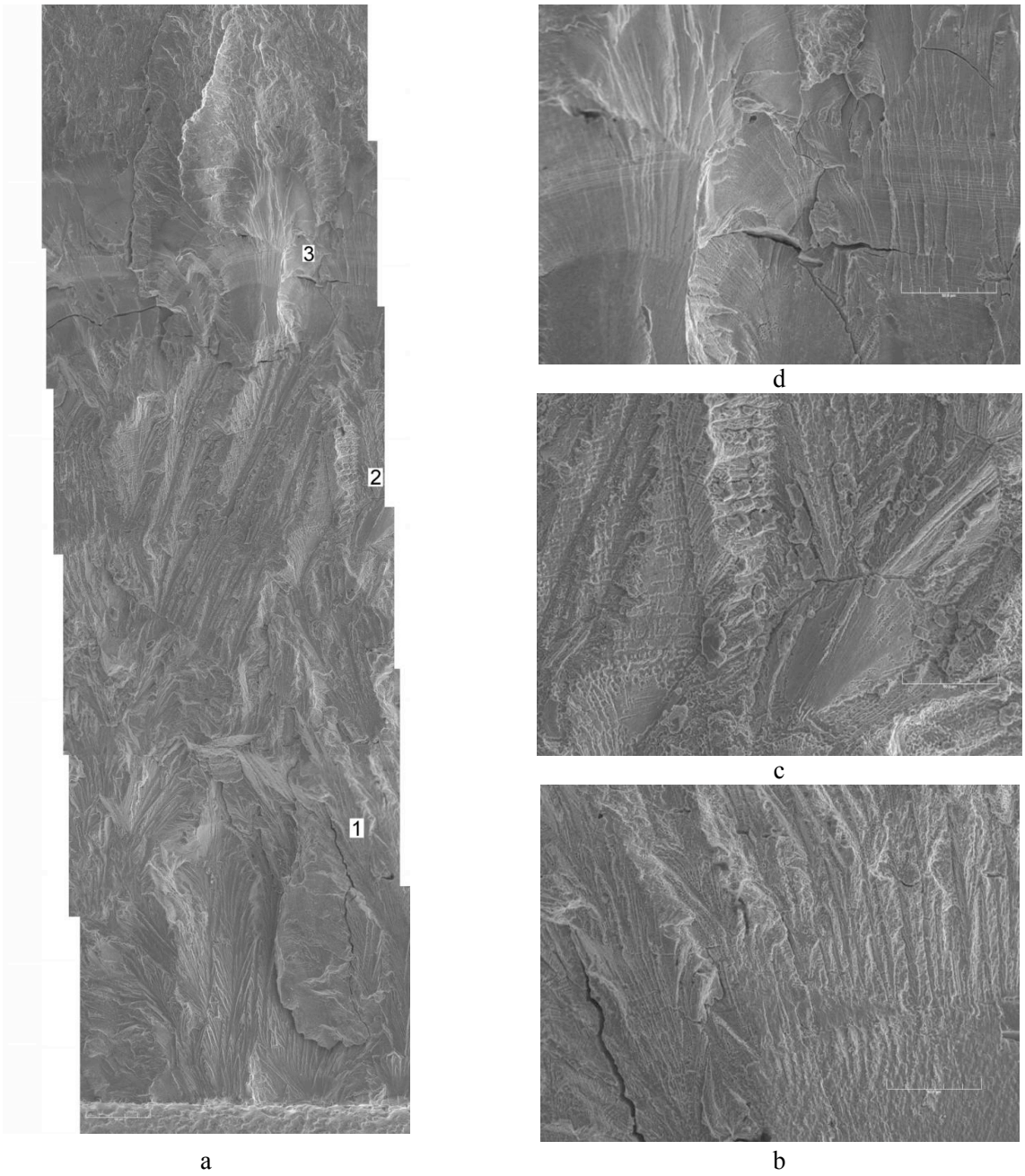

Figure 17. Micrographs showing (a) a slice of the entire length of fracture surface, and (b), (c), and (d) high–magnification micrographs of the fracture surface at locations 1, 2, and 3, respectively.

3.1.2 Specimen 85–3A–TT of the HAZ from Laboratory–Prepared SMA Weld, Test CGR-11

The environmental and loading conditions, experimental CGRs, allowed values of K_{max} from the K/size criterion, and deviation of applied K_{max} from the allowed value are given in Table 4 for Specimen 85–3A–TT. The test was started in a high–DO environment (e.g., effluent DO level of ≈600 ppb); the water flow rate was maintained constant at ≈105 mL/min during the test. The effluent

Table 4. Crack growth results for Specimen 85–3A–TT[a] of nonirradiated Type 304 SS SMA weld HAZ in high–purity water at 289°C.

Test Period[b]	Test Time, h	Cond.,[c] µS/cm	ECP[c] mV (SHE) Pt	ECP[c] mV (SHE) Steel	R Load Ratio	Rise Time, s	Down Time, s	Hold Time, s	K_{max}, MPa·m$^{1/2}$	ΔK, MPa·m$^{1/2}$	Growth Rate, m/s	Allowed K_{max}, MPa·m$^{1/2}$	Deviation in K_{max}[d], %
Pre a	144	0.10	183	27	0.21	0.50	0.50	0	16.13	12.74	5.46E-08	15.7	3
Pre b	148	0.08	182	32	0.21	0.50	0.50	0	15.01	11.86	5.00E-08	15.4	-2
1	166	0.07	182	32	0.51	30	2	0	14.64	7.18	5.61E-11	15.3	-5
2	190	0.07	184	41	0.51	30	2	0	16.73	8.20	5.50E-10	15.3	9
3	215	0.07	182	45	0.71	30	2	0	16.90	4.90	3.16E-11	15.3	11
4*	264	0.07	184	60	0.71	30	2	0	19.82	5.75	8.85E-10	15.1	32
5a*	298	0.07	188	68	0.71	300	2	0	19.80	5.74	2.75E-10	15.0	32
5b*	338	0.07	187	79	0.71	300	2	0	20.24	5.87	7.91E-10	14.8	36
6*	384	0.07	188	87	0.70	1000	2	0	20.51	6.15	4.57E-10	14.7	39
7	478	0.07	192	106	0.70	12	12	3600	21.15	0.00	6.60E-10	14.4	47
8	646	0.14	-482	-633	0.70	12	12	3600	21.37	0.00	9.13E-11	14.3	49
9	862	0.12	-477	-621	0.70	12	12	3600	24.96	0.00	4.29E-11	14.2	76

[a]Grand Gulf H5 SA weld bottom shell HAZ, nonirradiated.
[b]An asterisk indicates environmental enhancement of growth rates under cyclic loading.
[c]Represents values in the effluent. Water flow rate was maintained at ≈105 mL/min; the DO level in the effluent was ≈600 ppb during the high–DO test and <40 ppb during the low–DO test.
[d]Based on flow stress.

water conductivity and ECPs of a Pt and SS electrode were monitored continuously; the values are listed in the table. The effluent DO level was measured periodically.

Precracking was initiated at R ≈0.2, K_{max} ≈14 MPa m$^{1/2}$, and a triangular waveform. After ≈0.4 mm advance, R was increased incrementally to 0.7, and the waveform changed to a slow/fast sawtooth with rise times of 30–1000 s; in all cases time to unload was 2 s. The constant load tests were conducted using a trapezoidal waveform with R = 0.7, hold period at peak load of 1–h, and unload and reload periods of 12 s. During each test period, the maximum stress intensity factor K_{max} was maintained approximately constant by periodic load shedding (less than 2% decrease in load at any given time).

After ≈480 h, the DO level in the feedwater was decreased from ≈600 ppb to <40 ppb by sparging the feedwater tank with pure N_2. The changes in crack length and ECP of Pt and SS electrodes during the transient period are shown in Fig. 18. For this test, because the flow rate was higher than the rate used for the in–cell tests, changes in the environment were significantly faster. However, the changes in the steel ECP were slower than that in the Pt ECP, e.g., the ECP decreased below –400 mV (SHE) within 10 h for the Pt electrode and 40 h for the steel electrode. A slight increase in ECP values of both Pt and steel electrode at ≈530 h was due to an increase in the effluent DO level.

After the test, the final crack front was marked by fatigue cycling in air at room temperature. A detailed metallographic evaluation of the specimen was performed to examine the fracture surface and fracture plane morphologies. A 1–mm–thick slice of the entire CT specimen was cut off, and the remainder of the specimen was pulled apart. Photomicrographs of the fracture surface of the two halves of the broken specimen are shown in Fig. 19; a composite micrograph of the cross section of the specimen is shown in Fig. 20. The crack lengths were measured by both optical and scanning electron microscopy. The actual final crack extension was ≈40% greater than the value determined from the DC potential measurements. Crack extensions estimated from the DC potential drop method were scaled proportionately; the corrected values of K_{max} and growth rates are listed in Table 4.

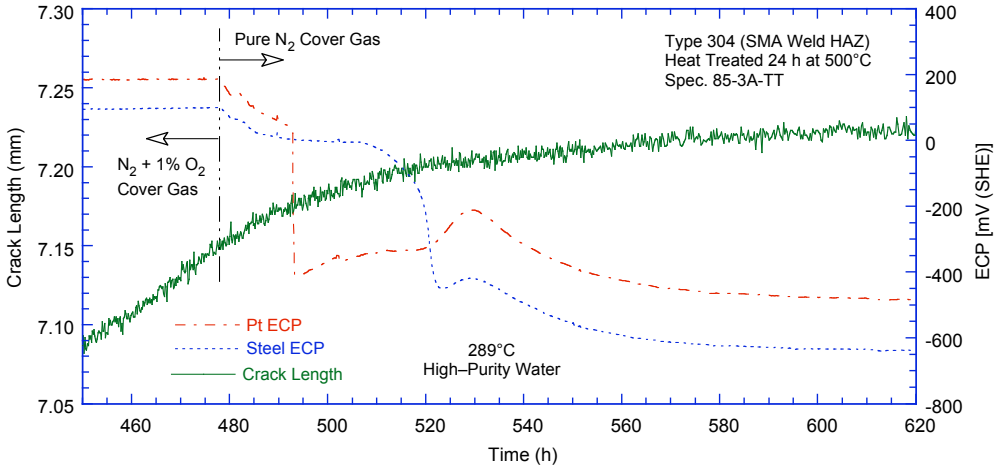

Figure 18. Change in crack length and ECP of Pt and SS electrodes during test periods 6–8 and the intermediate transition period.

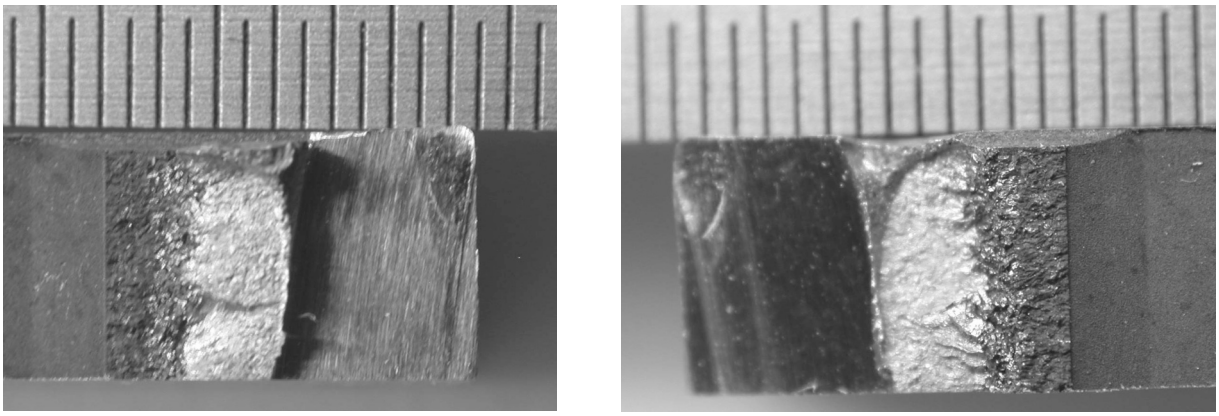

(a) (b)

Figure 19. Photomicrographs of the fracture surfaces of the two halves of Specimen 85–3A-TT.

The changes in crack length and K_{max} with time during the various test periods are shown in Figs. 21a–d. For this specimen, significant environmental enhancement occurred after ≈210 h when K_{max} was increased from ≈17 to 20 MPa $m^{0.5}$, Fig. 19b. Also, the results in Table 4 indicate that for this specimen, the loading condition during precracking and up to test period 3 satisfies the K/size criterion of Eq. 13, and is ≈34% higher than the allowed value for periods 4–6, 48% higher for period 7 and 8, and 76% higher for period 9.

The fracture plane orientation shown in Fig. 20 suggests that the applied K_{max} during test periods 7–9 may have exceeded the K/size criterion. The fracture plane is initially normal to the stress axis, but for the last ≈0.6–mm crack extension, it is at 45° to the stress axis. The change in the fracture plane orientation occurred at an average crack extension of 1.16 mm; actual values varied ≈1.0–1.25 mm across the thickness of the specimen. Also, the fracture surface morphology is predominantly TG along the plane normal to stress axis and completely IG along the plane 45° to stress axis. A micrograph of the fracture surface for Specimen 85–3A-TT is shown in Fig. 22, where a relatively straight crack front is observed.

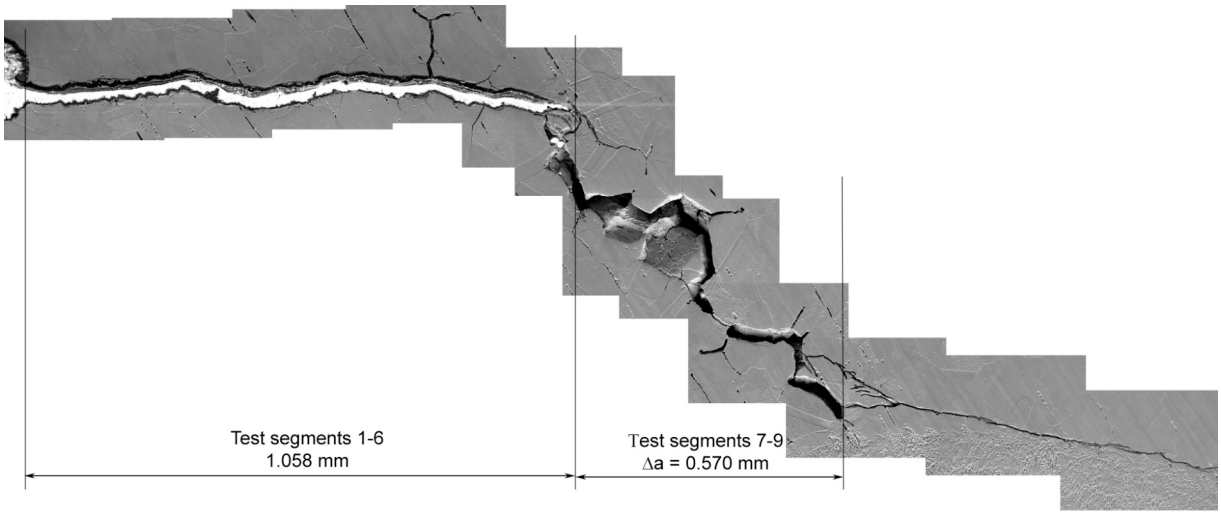

Figure 20. Micrograph of the cross section of Specimen 85-3A-TT showing the fracture plane profile.

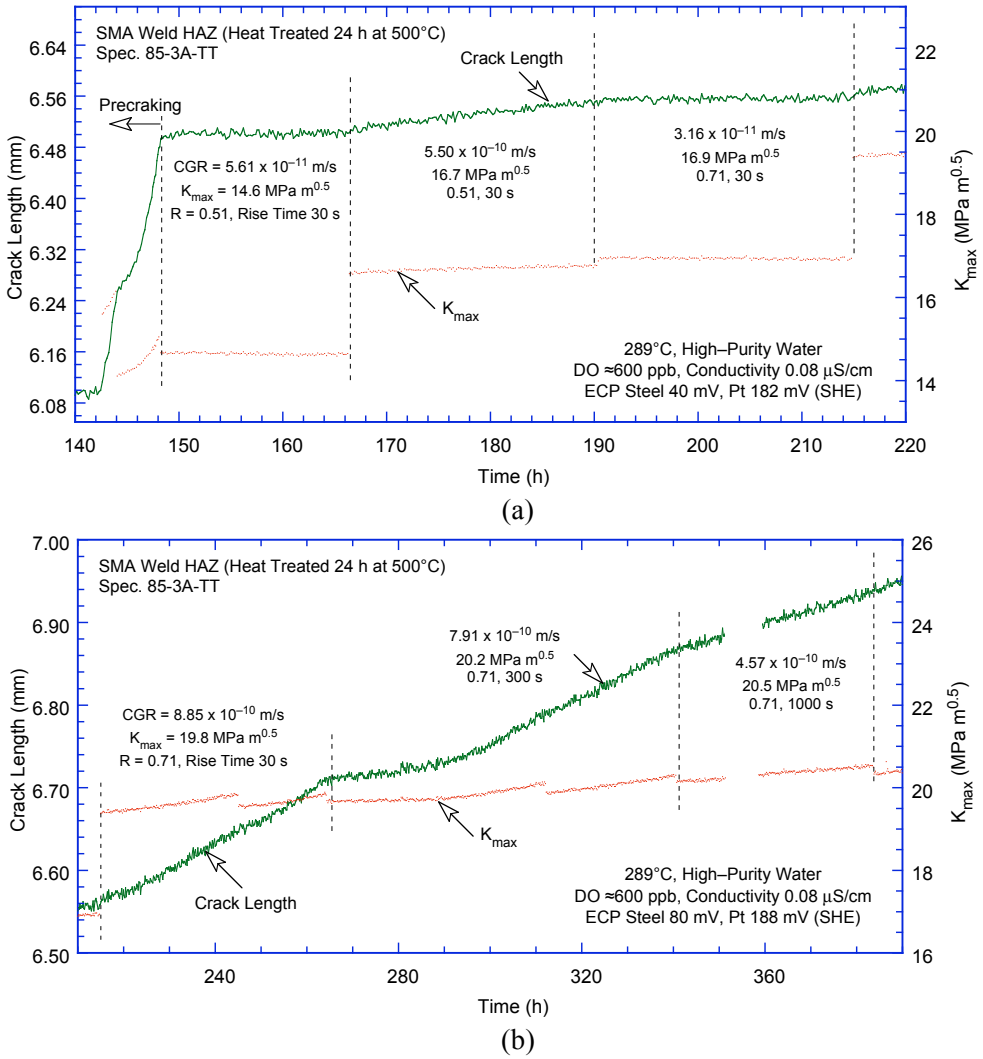

Figure 21. Crack–length–vs.–time plots for nonirradiated Type 304L bottom shell HAZ from the GG H5 weld in high–purity water at 289°C during test periods (a) 1–3, (b) 4-6, (c) 7–8, and (d) 9.

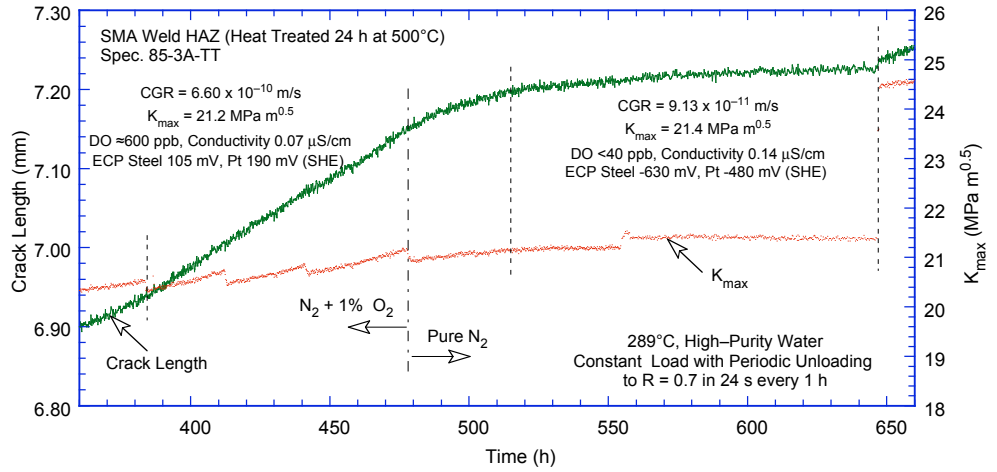

(c)

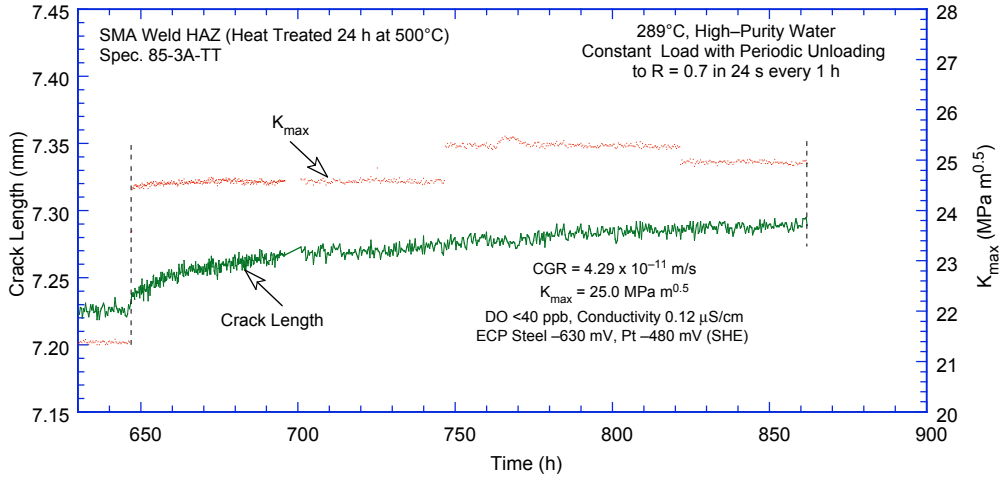

(d)

Figure 21. (Contd.)

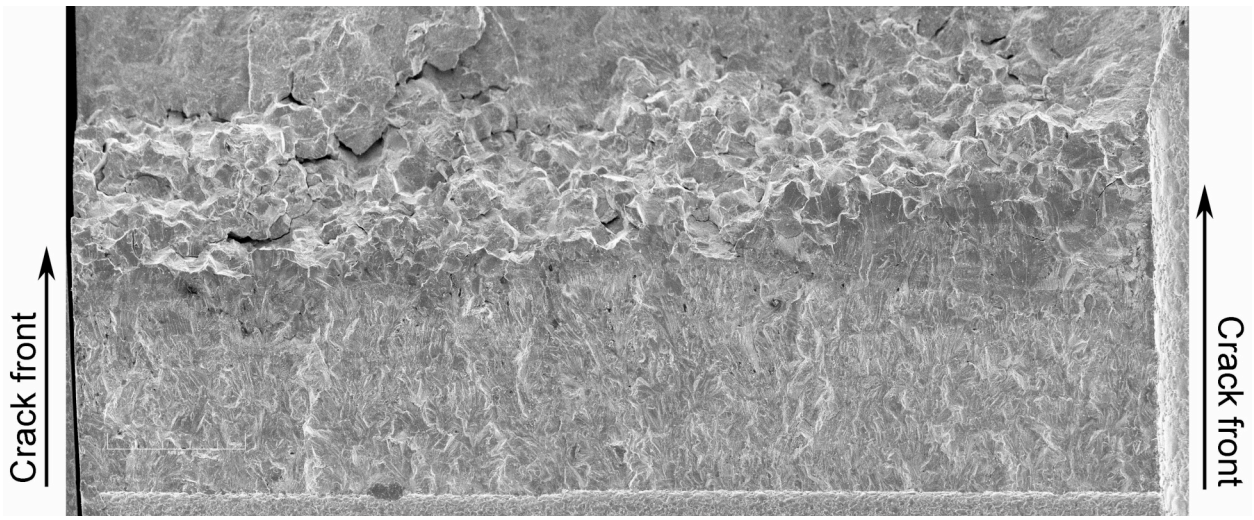

Figure 22. Micrograph of the fracture surface of Specimen 85-3A-TT tested in high–DO water at 289°C.

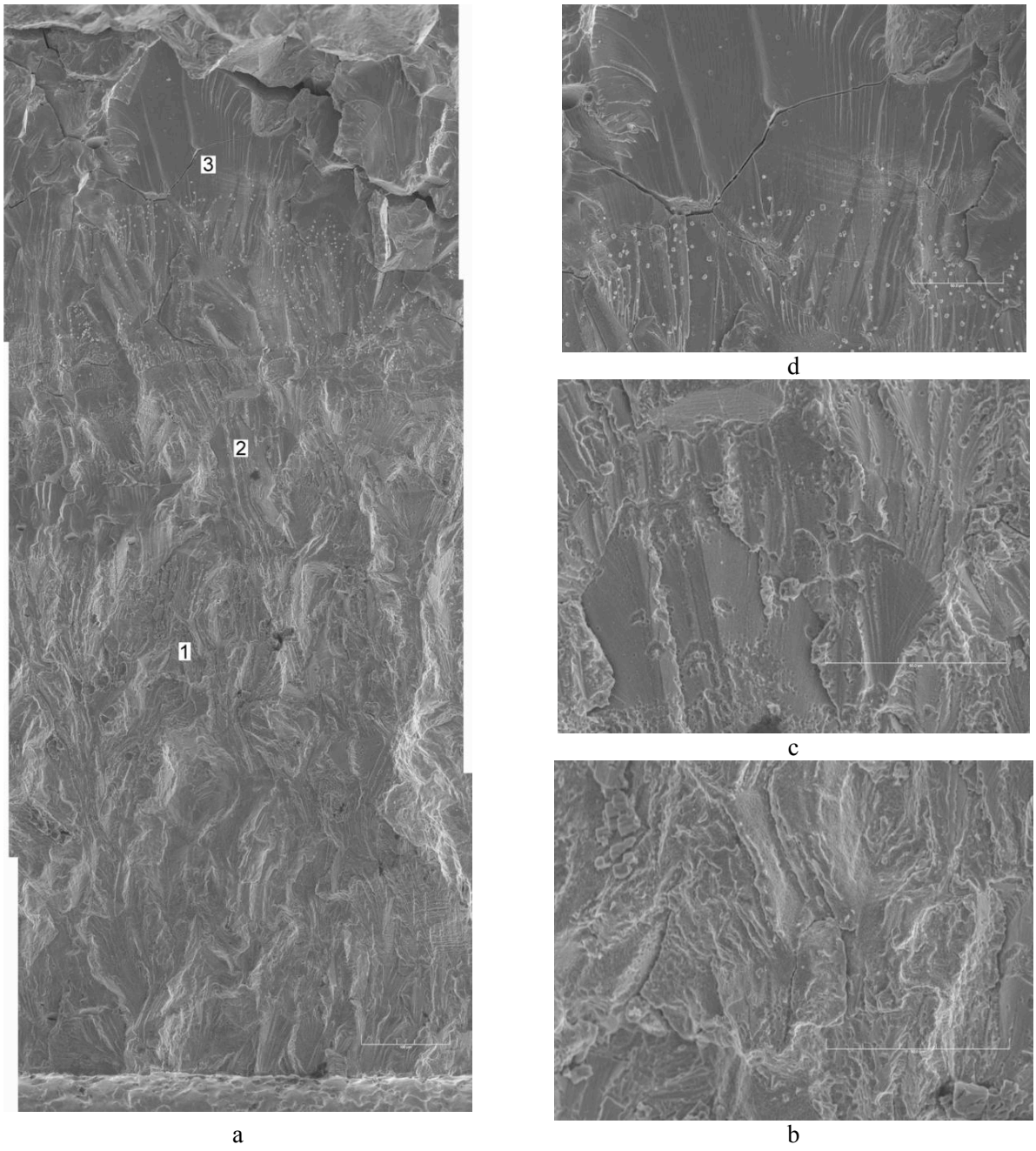

Figure 23. Micrograph showing (a) a slice of the fracture surface that was perpendicular to the stress axis, and (b), (c), and (d) high–magnification micrographs of the fracture surface at locations 1, 2, and 3, respectively.

The specimen was cleaned chemically to remove the surface oxide film before micrographic examination. Figure 23 presents micrographs of a slice of the fracture surface that is normal to the stress axis and shows typical fracture morphologies at select locations on the surface. The fracture surface exhibits a predominantly TG fracture morphology, and most of the TG facets show a well–defined river pattern (Fig. 23c, d). A narrow region of IG fracture appears before the fracture plane orientation changes along the plane 45° to the stress axis. Typical fracture morphologies along the change in the fracture plane orientation and before and after the change are shown in Fig. 24.

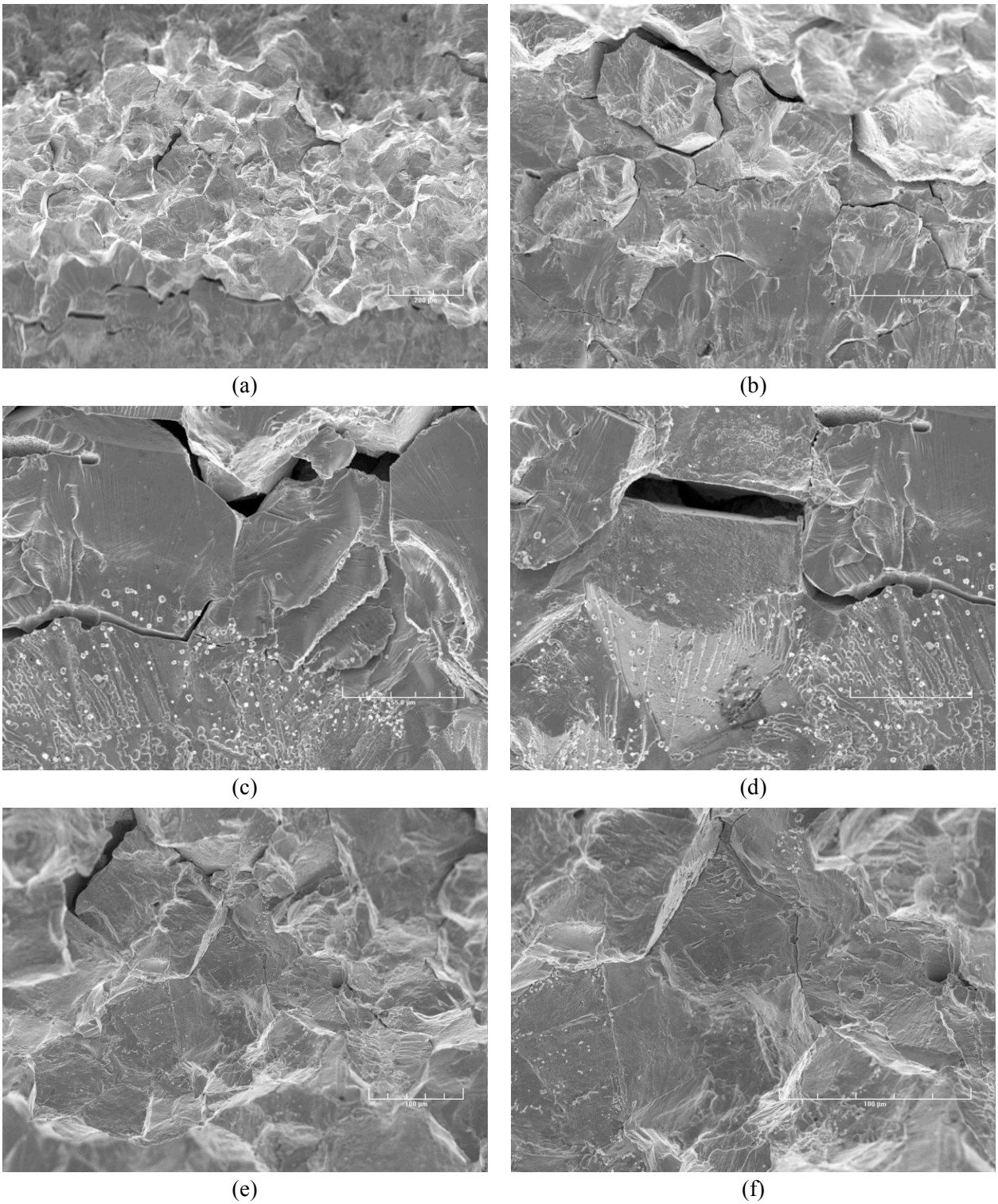

Figure 24. Typical fracture morphologies (a, b) along the change in the fracture plane direction and (c, d) before and (e, f) after the change in direction.

3.1.3 Specimen GG3B–A–TT of the HAZ from Grand Gulf Core Shroud H5 SA Weld, Test CGR-14

The environmental and loading conditions, experimental CGRs, allowable values of K_{max} by the K/size criterion of Eq. 13, and the deviation of applied K_{max} from the allowable value are given in Table 5 for Specimen GG3B–A–TT. During most test periods, K_{max} was maintained approximately constant by periodic load shedding. The test was started in high–DO water (≈400 ppb DO in effluent) and water flow rate of ≈100 mL/min. The effluent water conductivity and ECPs of a Pt and SS electrode were monitored continuously; the values are listed in the table. The effluent DO level was measured periodically.

Table 5. Crack growth results for Specimen GG3B–A–TT[a] of Type 304L HAZ in high–purity water at 289°C.

Test Period[b]	Test Time, h	Cond.,[c] µS/cm	ECP[c] mV (SHE) Pt	ECP[c] mV (SHE) Steel	R Load Ratio	Rise Time, s	Down Time, s	Hold Time, s	K_{max}, MPa·m$^{1/2}$	ΔK, MPa·m$^{1/2}$	Growth Rate, m/s	Allowed K_{max}, MPa·m$^{1/2}$	Deviation in K_{max}[d], %
Pre a	120	0.10	181	20	0.31	0.5	0.5	0	14.32	9.88	7.71E-09	14.4	-1
Pre b	143	0.09	185	25	0.31	5	5	0	14.41	9.95	5.91E-09	14.3	1
Pre c	238	0.08	192	36	0.51	1	1	0	15.02	7.36	1.34E-09	13.9	8
1a*	275	0.07	192	40	0.71	12	2	0	15.95	4.63	8.66E-10	13.9	15
1b*	305	0.07	193	42	0.71	12	2	0	16.31	4.73	2.50E-09	13.7	19
2*	328	0.07	194	44	0.71	30	2	0	16.49	4.78	1.22E-09	13.5	22
3*	403	0.07	195	53	0.70	300	2	0	16.66	5.00	2.80E-10	13.4	24
4*	522	0.07	198	65	0.70	1,000	12	0	16.65	5.00	1.12E-10	13.4	24
5a	580	0.07	203	79	0.70	12	12	3600	16.37	4.91	4.34E-11	13.4	22
5b	765	0.14	202	87	0.70	12	12	3600	16.66	5.00	9.60E-12	13.2	27
6	1,000	0.07	155	42	0.70	500	12	3600	18.52	5.56	9.06E-12	13.1	41
7	1,094	0.07	155	47	0.70	500	12	3600	20.38	6.11	4.47E-12	13.1	55

[a]Nonirradiated Grand Gulf H5 SA weld bottom shell HAZ, as–welded plus thermally treated for 24 h at 500°C.
[b]An asterisk indicates environmental enhancement of growth rates under cyclic loading.
[c]Represents values in the effluent. Water flow rate was ≈100 mL/min; the DO level in the effluent was ≈400 ppb.
[d]Based on flow stress.

Precracking was initiated at R ≈0.3, K_{max} ≈14 MPa m$^{1/2}$, and a triangular waveform. After ≈0.4–mm advance, R was increased incrementally to 0.7, and the waveform changed to a slow/fast sawtooth with rise times of 12–1000 s; in all cases, time to unload was 2 s. The constant load tests were conducted using a trapezoidal waveform with R = 0.7, hold period at peak load of 1–h, and unload and reload periods of 12 s. The test was interrupted twice, once at ≈240 h when the hydraulic pump tripped because of an increase in cooling water temperature, and again at 580 h when a power bump caused the hydraulic system to trip. Each time the test was restarted under the loading conditions prior to the interruption. The test conditions, e.g., crack length and growth rates, prior to the interruption were restored after the first restart but not the second restart. The specimen was accidentally overstrained during the second interruption; the crack length increased by ≈0.13 mm after the restart, and the growth rate was a factor of ≈5 lower. To help restore the higher growth rates, a 500–s rise time was added to the loading cycle but with no success. The unusually low CGRs measured during test periods 5b–7 may have been influenced by the accidental overstrain.

After the test, the final crack front was marked by fatigue cycling in air at room temperature. A detailed metallographic evaluation of the specimen was performed to examine the fracture surface and fracture plane morphologies. A 1–mm–thick slice of the entire CT specimen was cut off, and the remainder of the specimen was pulled apart. Composite micrographs of the cross section of the specimen and the fracture surface of the specimen are shown in Figs. 25 and 26, respectively.

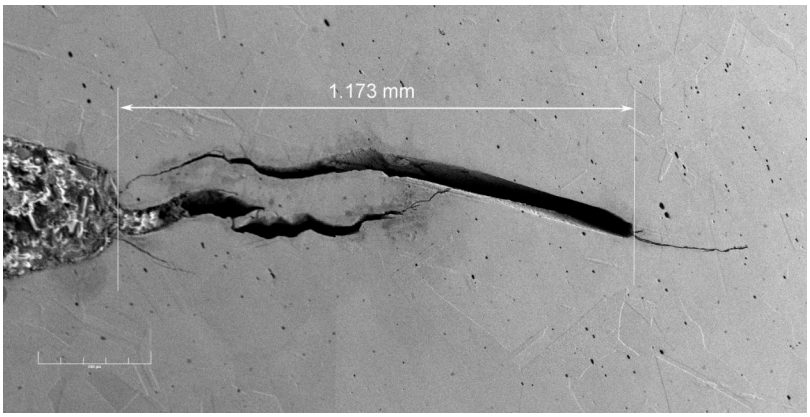

Figure 25. Micrograph of the cross section of Specimen GG3B-A-TT showing the fracture plane profile.

In Specimen GG3B–A–TT, fracture seems to have occurred along two planes. These two fracture planes overlap in the specimen cross section shown in Fig. 25. Also, note that the crack extension represented by the noncorroded fine cracks on the right occurred during fatigue cycling at room temperature to mark the final crack front. The final crack extension, measured by scanning–electron microscopy, was ≈30% greater than the value determined from the DC potential measurements. Crack extensions estimated by the DC potential drop method were scaled proportionately; the corrected values of K_{max} and growth rates are listed in Table 5.

The changes in crack length and K_{max} with time during the various test periods are shown in Figs. 27a–c. For this specimen, significant environmental enhancement occurred after ≈270 h when R was increased from 0.5 to 0.7, Fig. 27b. Also, the results in Table 5 indicate that for this specimen, the K values during precracking and up to test period 5 were 15–27% higher than the K/size criterion of Eq. 13, and 40–55% higher than the allowed value for periods 6 and 7.

Micrographs showing a slice of the entire crack extension and typical fracture morphology at select locations on the surface are shown in Fig. 28a–d. This specimen was not cleaned chemically to remove the surface oxide film. Once again, a predominantly TG fracture morphology is observed for the entire crack extension. Most of the TG facets show the well–defined river pattern.

Figure 26. Micrograph of the fracture surface of Specimen GG3B-A-TT tested in high–DO water at 289°C.

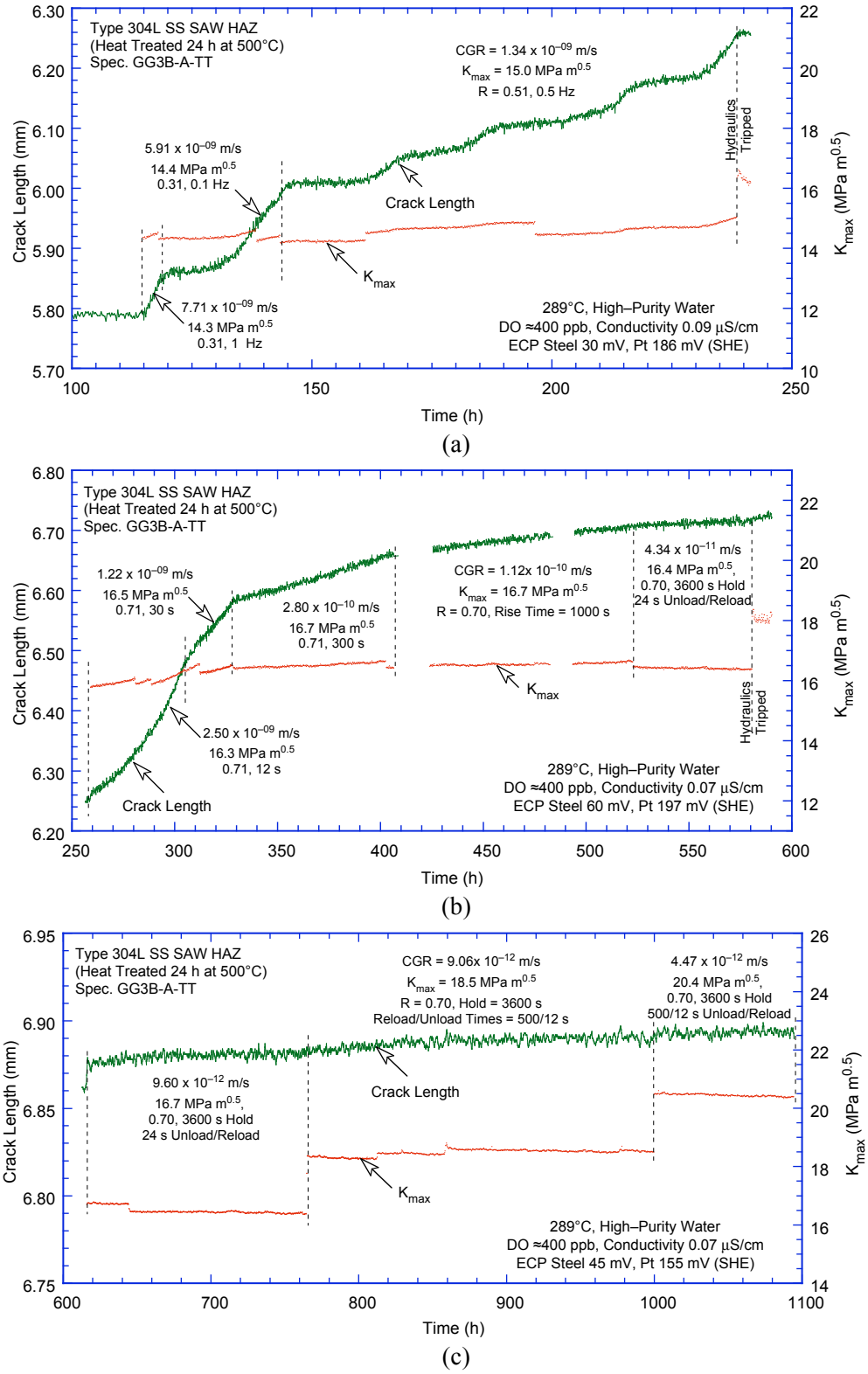

Figure 27. Crack–length–vs.–time plots for nonirradiated thermally–treated Type 304L bottom shell HAZ from the Grand Gulf H5 SA weld in high–purity water at 289°C during test periods (a) precracking, (b) 1-5a, and (c) 5b–7.

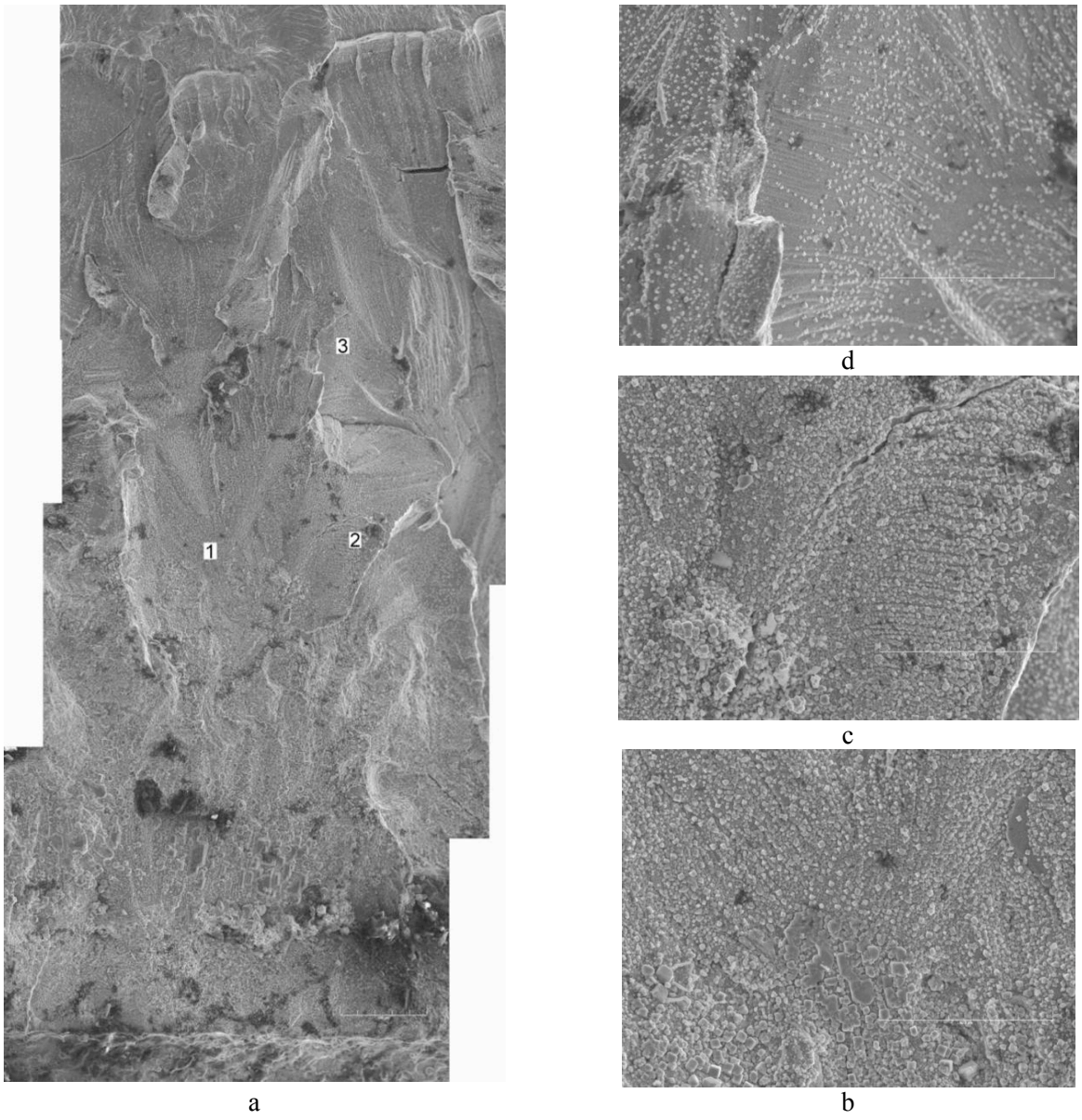

Figure 28. Micrographs showing (a) a slice of the entire length of the fracture surface, and (b), (c), and (d) high–magnification micrographs of the fracture surface at locations 1, 2, and 3, respectively.

3.1.4 Specimen 85–YA of the HAZ from Laboratory–Prepared SMA Weld, Test CGR-22

This test was conducted with the in–cell test facility, although the specimen (85–YA) was not irradiated. The environmental and loading conditions, experimental CGRs, allowed values of K_{max} from the K/size criterion, and deviation of applied K_{max} from the allowed value are given in Table 6. The test was started in a high–DO environment (e.g., effluent DO level of ≈300 ppb); the water flow rate was maintained constant at ≈22 mL/min during the test. The system was operated for about a week for the environmental conditions to stabilize. Because of a faulty ECP cell temperature controller, the ECPs of the Pt and SS electrodes in the effluent could not be monitored during the test. The effluent DO level was measured periodically.

Table 6. Crack growth results for Specimen 85–YA[a] of nonirradiated Type 304 SS SMA weld HAZ in high–purity water at 289°C.

Test Period[b]	Test Time, h	ECP[c] mV (SHE) Pt	ECP[c] mV (SHE) Steel	O_2 Conc.,[d] ppb	R Load Ratio	Rise Time, s	Down Time, s	Hold Time, s	K_{max}, MPa·m$^{1/2}$	ΔK, MPa·m$^{1/2}$	Growth Rate, m/s	Allowed K_{max}, MPa·m$^{1/2}$	Margin in K_{max},[e] %
Pre a	149	–	–	300	0.33	0.5	0.5	0	16.15	10.82	4.73E-08	15.8	2
Pre b	192	–	–	300	0.33	10	10	0	16.74	11.22	5.72E-09	15.4	9
1	263	–	–	300	0.52	300	12	0	16.66	8.00	2.19E-11	15.4	8
2	288	–	–	300	0.52	30	12	0	16.74	8.04	2.51E-10	15.4	9
3	318	–	–	300	0.52	30	12	0	19.22	9.23	6.21E-10	15.2	26
4*	384	–	–	300	0.51	300	12	0	19.31	9.46	3.68E-10	15.1	28
5*	551	–	–	300	0.51	1000	12	0	19.82	9.71	1.85E-10	14.9	33
6	768	–	–	300	1.00	–	–	–	19.74	0.00	negligible	14.9	32

[a]Laboratory–prepared Type 304 SS (Heat 10285) SMA weld HAZ, as–welded condition.
[b]An asterisk indicates environmental enhancement of growth rates under cyclic loading.
[c]Could not be measured because of faulty temperature controller
[d]Represents values in the effluent. Conductivity was ≈0.07 and 0.2 μS/cm in feedwater and effluent, respectively.
[e]Based on flow stress.

The specimen was fatigue precracked at R = 0.3, K_{max} = 15 MPa m$^{1/2}$, triangular waveform, and 1 Hz frequency. After ≈0.7–mm crack advance the test conditions were changed to R = 0.5, K_{max} = 15 and then 17 MPa m$^{1/2}$, and trapezoidal waveform with rise time of 30–1000 s and unload time of 12 s. During each test period, the maximum stress intensity factor K_{max} was maintained approximately constant by periodic load shedding (less than 2% decrease in load at any given time).

After the test, the final crack front was marked by fatigue cycling in air at room temperature. A detailed metallographic evaluation of the specimen was performed for the fracture surface and fracture plane morphologies. The EDM cutting facility was used to remove a thin slice of the fracture surface from the fractured CT specimen. A micrograph of the fracture surface is shown in Fig. 29. The final crack length was measured by scanning electron microscopy. The actual crack extension was ≈80% greater than the value determined from the DC potential measurements. Crack extensions estimated from the DC potential drop method were scaled proportionately; the corrected values of K_{max} and growth rates are listed in Table 6.

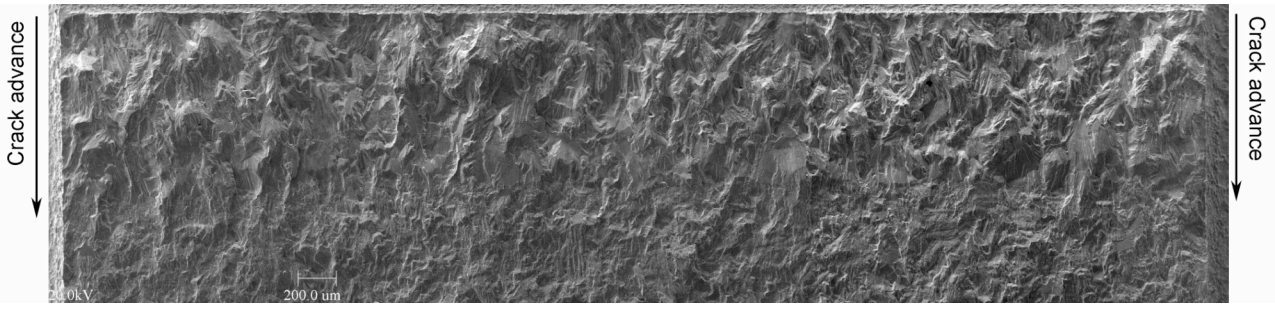

Figure 29. Micrograph of the fracture surface of Specimen 85–YA tested in BWR environment at 289°C.

The changes in crack length and K_{max} with time during the various test periods are shown in Figs. 30a–c. For this specimen, significant environmental enhancement occurred after ≈320 h when the rise time was increased from 30 to 300 s, Fig. 30b. Also, the results in Table 6 indicate that for this specimen, loading condition during precracking and up to test period 2 are ≈9% higher than the value allowed by the K/size criterion of Eq. 13 and is 26–32% higher for test periods 3–6.

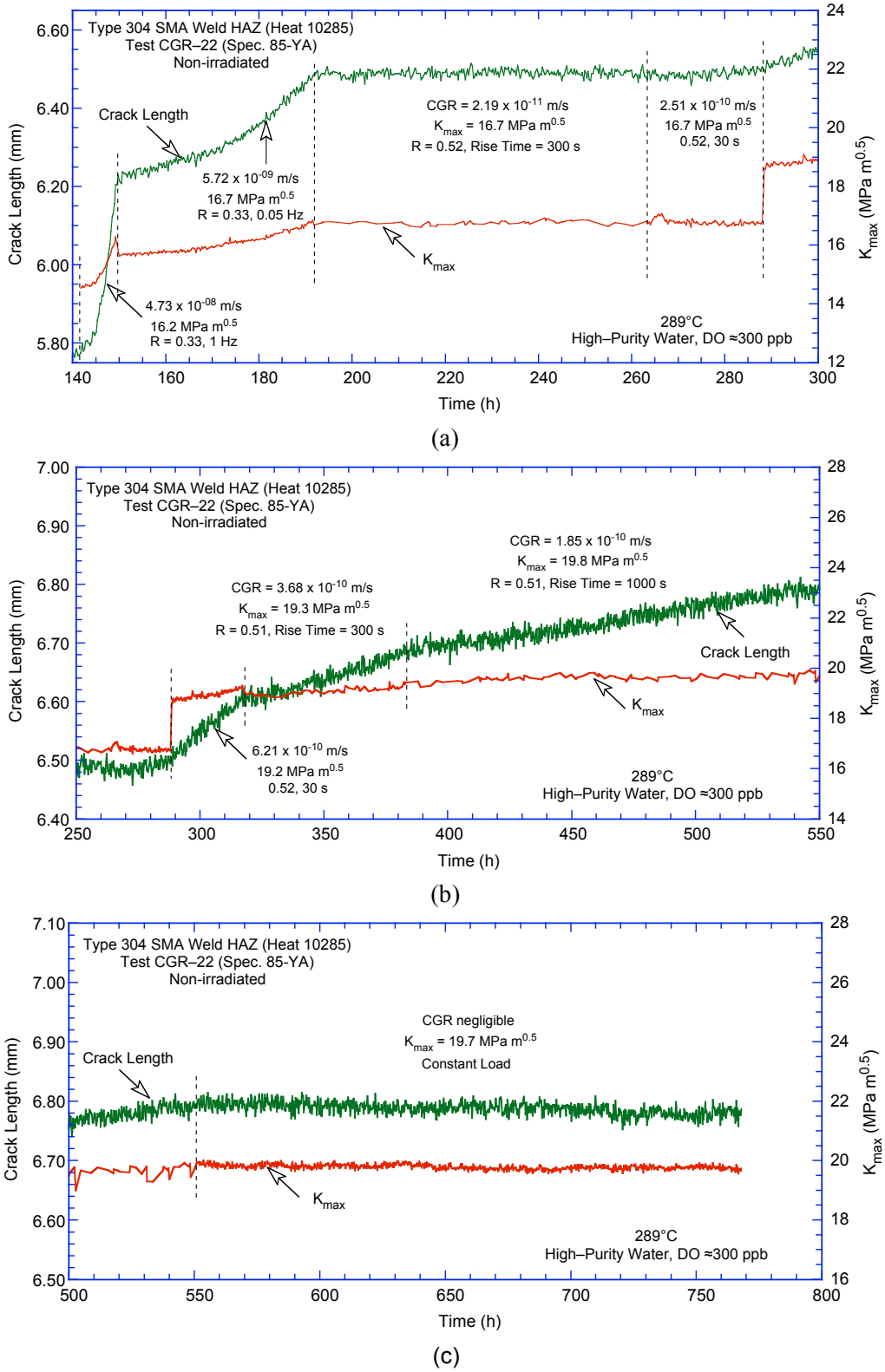

Figure 30. Crack–length–vs.–time plots for nonirradiated as–welded Type 304 SMA weld HAZ in high–purity water at 289°C during test periods (a) up to 2, (b) 3–5, and (c) 6.

Micrographs showing a slice of the entire crack extension and typical fracture morphology at select locations on the surface are shown in Fig. 31a–c. The fracture morphology is predominantly TG with terraced facets and a river pattern for most of the test (Fig. 31a) and changes to IG fracture near the end of the test during test periods 4 and 5 (Figs. 31c and d). Secondary cracks are also observed during these test periods.

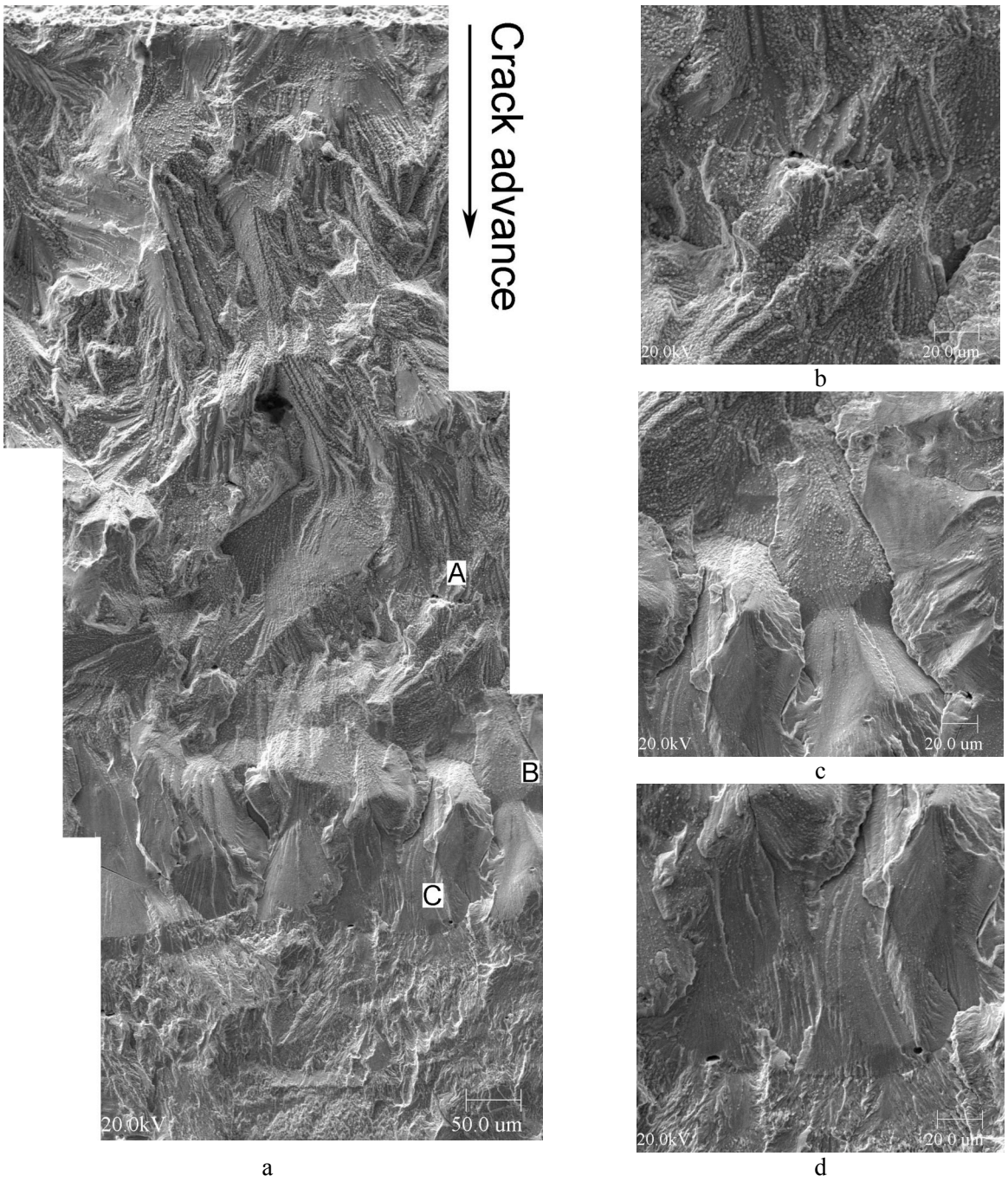

Figure 31. Micrograph showing (a) a slice of the entire length of the fracture surface and (b), (c), and (d) high–magnification micrographs of the fracture surface at locations A, B, and C, respectively.

3.2 Crack Growth Tests on Irradiated Stainless Steels in BWR Environments

Crack growth tests have been completed in BWR environments at 289°C on 1/4–T CT specimens of Types 304L and 304 SS HAZs irradiated to 5.0 x 10^{20} n/cm^2. The specimens for the tests were obtained from the top shell Type 304L SS HAZ of the GG core shroud H5 SA weld (Specimens GG5T–A and GG5T–B) and from the HAZ of a laboratory–prepared Type 304 SS SMA weld in two conditions, e.g., as–welded (Specimen 85–7A) and as–welded plus thermally treated for 24 h at 500°C (Specimen 85–1A–TT). The significant results for the various tests are summarized below.

3.2.1 Specimen GG5T–A of Type 304L SS HAZ Irradiated to 5.0 x 10^{20} n/cm^2

The Specimen GG5T–A test was started in high–purity water with ≈250 ppb DO and ≈10 mL/min flow rate. The environmental and loading conditions, experimental CGRs, the allowed K_{max} from K/size criterion, and the margin between the applied K_{max} and the allowed value are given in Table 7. The changes in crack length and K_{max} with time during various test periods are shown in Fig. 32. Precracking was carried out at R ≈ 0.2–0.3, K_{max} = 12.5–13.5 MPa m$^{1/2}$, and triangular waveform with 1 Hz frequency. After ≈0.2–mm extension, R was increased incrementally to 0.7, and the loading waveform changed to a slow/fast sawtooth with rise times of 60–1000 s. For this specimen, environmental enhancement occurred after ≈200 h during test period 3b, Fig. 32a.

Table 7. Crack growth results for Specimen GG5T–A[a] of Type 304L HAZ in high–purity water at 289°C.

Test Period[b]	Test Time, h	ECP[c] mV (SHE) Pt	ECP[c] mV (SHE) Steel	O_2 Conc.,[c] ppb	R Load Ratio	Rise Time, s	Down Time, s	Hold Time, s	K_{max}, MPa·m$^{1/2}$	ΔK, MPa·m$^{1/2}$	Growth Rate, m/s	Allowed K_{max}, MPa·m$^{1/2}$	Margin in K_{max},[d] %
1	69	212	205	250	0.17	0.5	0.5	0	12.4	10.3	1.71E-08	28.1	-56
2a	74	212	205	250	0.28	0.5	0.5	0	12.3	8.9	3.11E-09	28.0	-56
2b	144	214	201	250	0.30	0.5	0.5	0	12.8	8.9	2.70E-09	28.0	-54
2c	165	214	201	250	0.32	0.5	0.5	0	13.5	9.2	1.06E-08	27.8	-51
3a	194	213	195	250	0.52	60	4	0	14.3	6.9	4.30E-11	27.8	-49
3b*	215	213	195	250	0.52	60	4	0	15.3	7.4	1.61E-09	27.6	-45
4*	260	209	196	250	0.69	300	4	0	14.7	4.6	3.34E-10	27.5	-47
5*	305	207	196	250	0.69	1000	12	0	14.7	4.6	3.89E-10	27.4	-46
6	355	206	196	250	0.70	60	12	0	15.3	4.6	3.01E-11	27.3	-44
7	378	205	199	250	0.71	60	12	0	16.6	4.8	8.03E-11	27.2	-39
8	482	199	193	250	0.51	30	4	0	16.6	8.1	8.57E-11	27.2	-39

[a]Grand Gulf H5 SA weld top shell HAZ, irradiated to 5.0 x 10^{20} n cm^{-2}.
[b]An asterisk indicates environmental enhancement of growth rates under cyclic loading.
[c]Represents values in the effluent. Conductivity was ≈0.07 and 0.2 µS/cm in feedwater and effluent, respectively.
[d]Based on flow stress.

After 305 h, the specimen was overstrained to ≈16.5 MPa m$^{1/2}$ due to a power bump. Although the loading systems are interlocked to shut down in case of a power failure, for the small specimens used in the irradiated tests, the internal pressure is sufficient to overload the specimen. The enhanced growth rates observed prior to the interruption could not be restored even after K_{max} was increased to 16.6 MPa m$^{1/2}$. The crack may have side branched due to overstrain, and the crack length and loading conditions may no longer be accurately characterized; therefore, the test was terminated after ≈480 h. Post–test measurements of the final crack front were not performed for this specimen. The specimen is intact and could potentially be used to continue the CGR test.

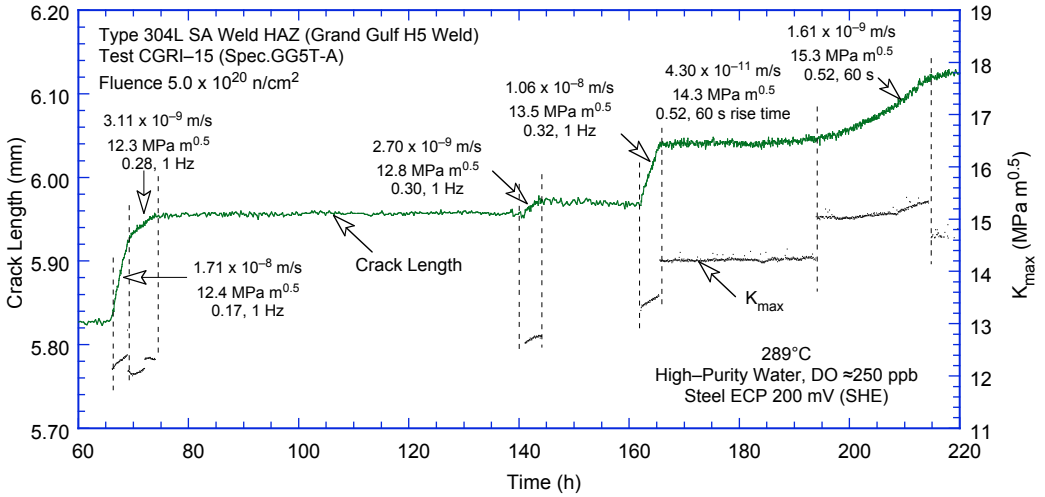

(a)

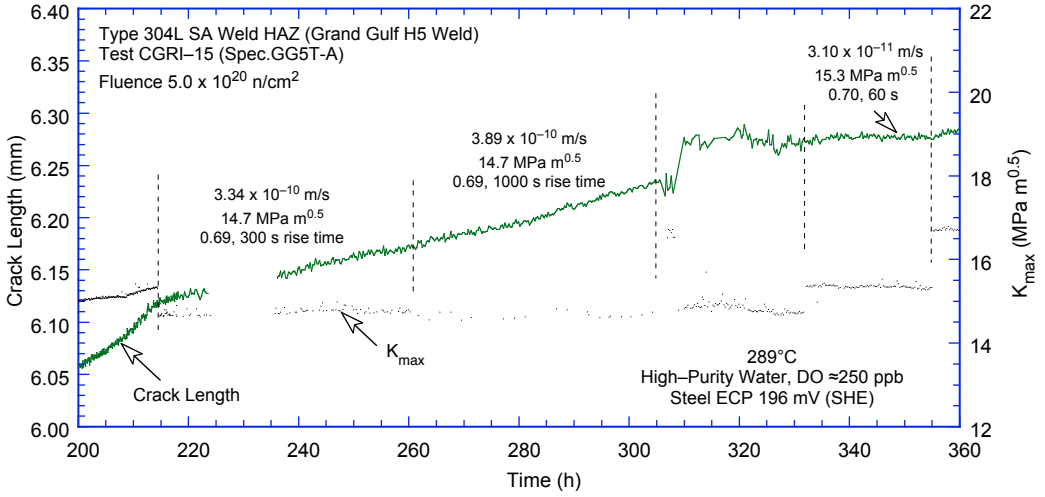

(b)

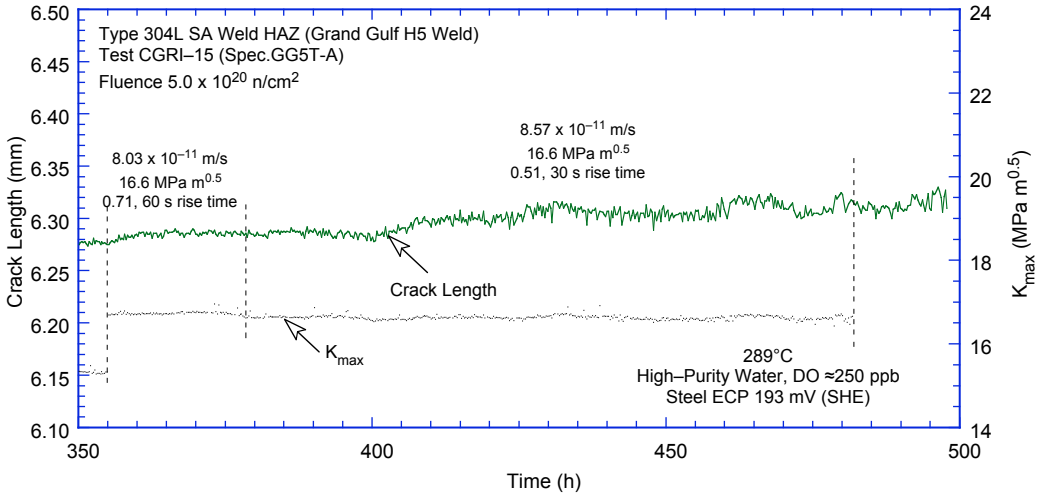

(c)

Figure 32. Crack–length–vs.–time plots for irradiated Grand Gulf H5 weld HAZ in high–purity water at 289°C during test periods (a) precracking–3, (b) 4–6, and (c) 7–8.

3.2.2 Specimen GG5T–B of Type 304L SS HAZ Irradiated to 5.0 x 10^{20} n/cm^2

The Specimen GG5T–B test was started in high–purity water with ≈350 ppb DO and ≈10 mL/min flow rate. The test conditions, experimental CGRs, the allowed K_{max} from K/size criterion, and the margin between the applied K_{max} and the allowed value are given in Table 8. The changes in crack length and K_{max} with time during various test periods are shown in Fig. 33. Precracking was carried out at R ≈ 0.2–0.3, K_{max} ≈ 13.0 MPa $m^{1/2}$, and triangular waveform with 1 Hz frequency. After ≈0.2–mm extension, R was increased to 0.5, and the loading waveform was changed to a slow/fast sawtooth with rise times of 30–300 s. Finally, R was increased to 0.7. For this specimen environmental enhancement occurred after ≈125 h during test period 2b, Fig. 33a.

Table 8. Crack growth results for Specimen GG5T–B[a] of Type 304L HAZ in high–purity water at 289°C.

Test Period[b]	Test Time, h	ECP,[c] mV (SHE) Pt	ECP,[c] mV (SHE) Steel	O_2 Conc.,[c] ppb	R Load Ratio	Rise Time, s	Down Time, s	Hold Time, s	K_{max}, MPa·$m^{1/2}$	ΔK, MPa·$m^{1/2}$	Growth Rate, m/s	Allowed K_{max}, MPa·$m^{1/2}$	Margin in K_{max},[d] %
Pre	81	225	211	350	0.20	0.50	0.5	0	13.8	11.0	7.24E-09	28.1	-51
1	105	218	200	350	0.30	0.50	0.5	0	13.0	9.1	4.59E-09	28.0	-54
2a	122	216	206	350	0.50	60	4	0	12.8	6.4	negligible	28.0	-54
2b*	154	214	199	350	0.51	30	4	0	14.4	7.1	9.13E-10	27.8	-48
3*	221	211	199	350	0.49	300	4	0	14.7	7.5	2.82E-10	27.6	-47
4*	296	204	200	350	0.70	300	4	0	14.8	4.4	2.35E-10	27.4	-46
5*	362	229	200	350	0.68	1,000	12	0	14.7	4.7	2.98E-10	27.2	-46
6	433	201	176	350	0.69	300	12	3,600	14.7	4.6	6.75E-10	26.7	-45
7	530	220	204	350	1.00	–	–	–	15.0	0.0	4.24E-10	26.4	-43
8	584	215	202	350	0.69	300	12	9,700	15.2	4.7	5.62E-10	26.1	-42
9	724	-532	-285	350	0.69	300	12	9,700	14.9	4.6	negligible	26.0	-43
10	893	-533	-530	350	0.69	300	12	–	15.0	4.6	negligible	26.0	-42

[a]Grand Gulf H5 SA weld top shell HAZ, irradiated to 5.0 x 10^{20} n cm^{-2}.
[b]An asterisk indicates environmental enhancement of growth rates under cyclic loading.
[c]Represents values in the effluent. Conductivity was ≈0.07 and 0.2 µS/cm in feedwater and effluent, respectively.
[d]Based on flow stress.

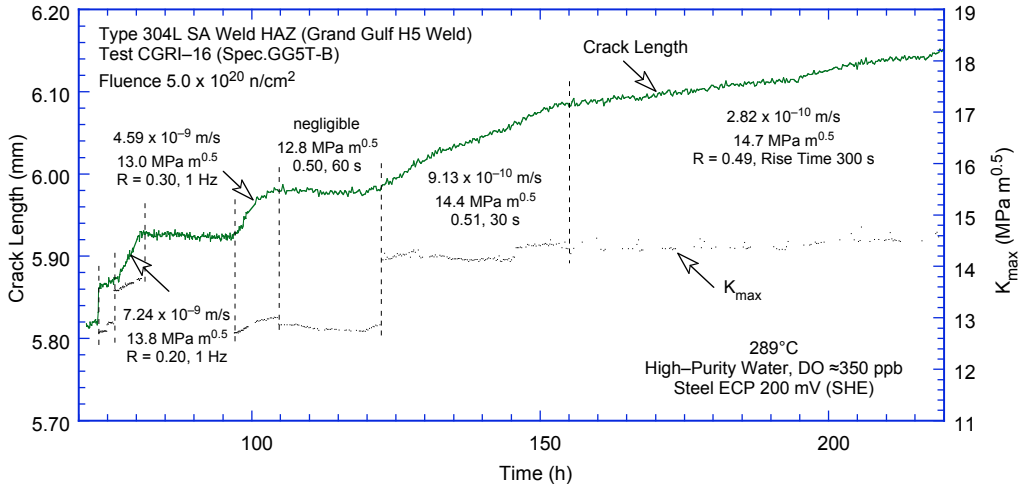

(a)

Figure 33. Crack–length–vs.–time plots for irradiated Grand Gulf H5 weld HAZ Specimen GG5T–B in high–purity water at 289°C during test periods (a) precracking–3, (b) 4–7, and (c) 8–10.

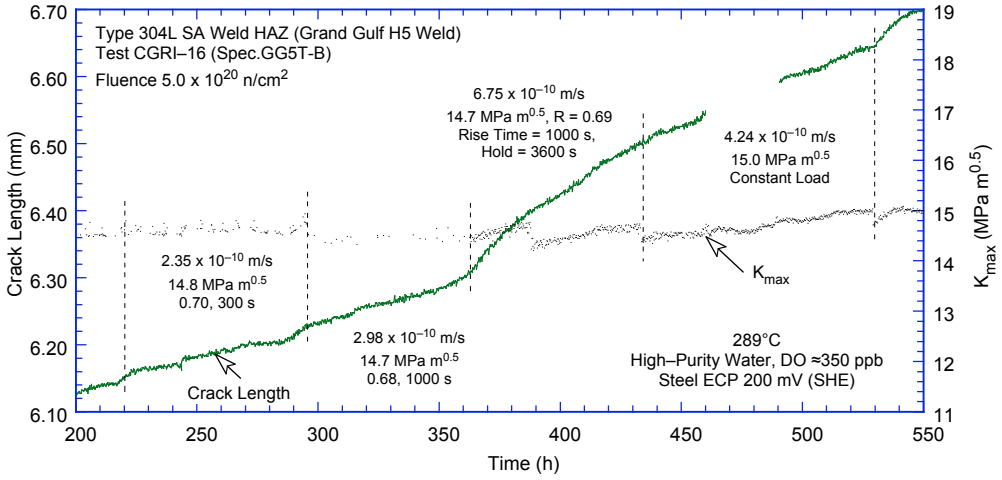

(b)

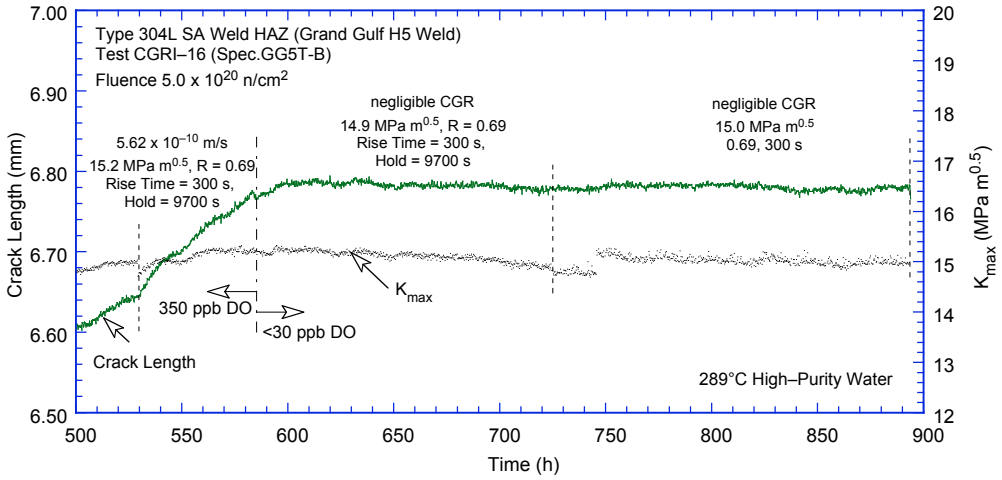

(c)

Figure 33. (Contd.)

After ≈575 h, the DO level in the feedwater was decreased from ≈350 ppb to <30 ppb by sparging the feedwater tank with N_2 plus 5% H_2 gas mixture. The change in crack length and ECP of Pt and SS electrodes during the transient periods is shown in Fig. 34. The change in ECP was relatively fast; the ECP decreased to –400 mV (SHE) in ≈5 h for the Pt electrode decreased to approximately –200 mV in 24 h and then gradually to –550 mV in the next ≈300 h for the SS electrode. In the low–DO environment, crack growth essentially stopped under both trapezoidal and saw–tooth loading waveforms.

After the test, the final crack size was marked by fatigue cycling at room temperature in air. The specimen was then fractured, and the fracture surface of both halves of the specimen was photographed with a telephoto lens through the cell window. A photomicrograph of the fracture surface of both halves of the specimen is shown in Fig. 35. The final crack length was measured from the photograph by the 9/8 averaging technique; the difference in measured and estimated crack lengths was <5%.

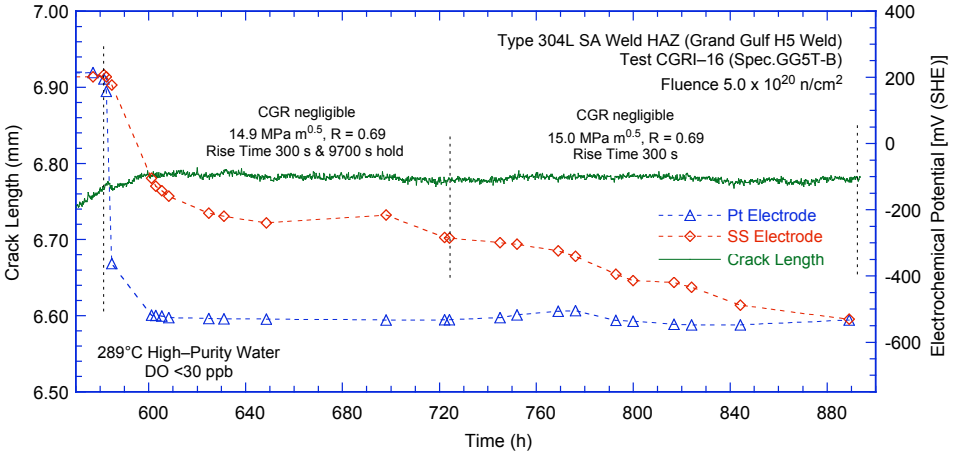

Figure 34. Change in crack length and ECP of Pt and SS electrodes when the DO level in feedwater was decreased from ≈350 to <30 ppb.

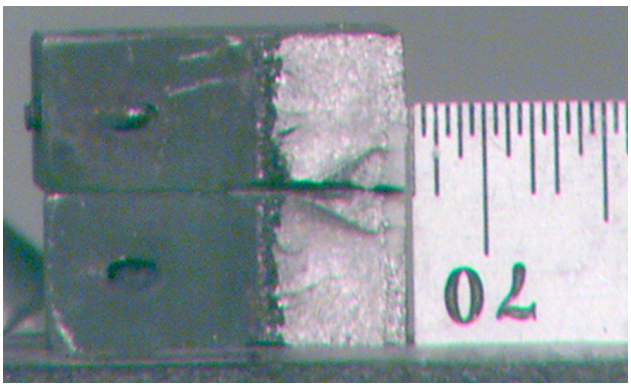

Figure 35.
Photomicrograph of the fracture surface of Specimen GG5T–B.

3.2.3 Specimen 85–1A–TT of Type 304 SS HAZ Irradiated to 5.0 x 10^{20} n/cm^2

The Specimen 85–1A–TT test was started in a high–purity water with ≈200 ppb DO and ≈10.0 mL/min flow rate. The test conditions, experimental CGRs, the allowed K_{max} from K/size criterion, and the margin between the applied and allowed values of K_{max} are given in Table 9.

Precracking was carried out at R ≈ 0.2, K_{max} ≈ 13.5 MPa m$^{1/2}$, and triangular waveform with 1 or 2 Hz frequency. After ≈0.25–mm extension, R was increased to 0.7, and the loading waveform changed to a slow/fast sawtooth with rise times of 60–1000 s. After ≈600 h the feedwater cover gas was changed from a mixture of N_2 + 1% O_2 to N_2 + 5% H_2. The changes in crack length and ECP of Pt and SS electrodes during the transient period are shown in Fig. 36. During test period 7, the ECP decreased to below –500 mV (SHE) within 10 h for the Pt electrode and decreased to below –200 mV (SHE) after ≈48 h for the SS sample. In low–DO water, the CGR, under the same loading condition, decreased by a factor of ≈5 relative to that in high–DO water.

After the CGR test was completed, a J–R curve test was performed on the same specimen at 289°C in high–purity water with ≈250 ppb DO. The test was conducted at a constant extension rate in accordance with ASTM specification E 1737 for "J–Integral Characterization of Fracture Toughness." The test was interrupted periodically (by holding the specimen at constant strain) to measure the crack length by the DC potential drop measurements. Specimen extension was monitored and controlled outside the high–temperature zone.

Table 9. Crack growth results for Specimen 85–1A–TT[a] of Type 304 SS SMA weld HAZ in high–purity water at 289°C.

Test Period[b]	Test Time, h	ECP,[c] mV (SHE) Pt	ECP,[c] mV (SHE) Steel	O_2 Conc.,[c] ppb	R Load Ratio	Rise Time, s	Down Time, s	Hold Time, s	K_{max}, MPa·m$^{1/2}$	ΔK, MPa·m$^{1/2}$	Growth Rate, m/s	Allowed K_{max}, MPa·m$^{1/2}$	Margin in K_{max},[d] %
Pre a	98	229	163	200	0.17	0.25	0.25	0	13.9	11.6	2.64E-08	30.5	-54
Pre b	101	228	161	200	0.24	0.50	0.50	0	13.3	10.1	2.10E-08	30.3	-56
1a	145	213	166	200	0.50	60	4	0	14.6	7.3	negligible	30.3	-52
1b*	217	203	175	200	0.50	1,000	4	0	15.1	7.6	4.80E-10	30.2	-50
2*	262	201	178	200	0.70	300	4	0	16.1	4.8	3.55E-10	29.9	-46
3*	314	199	172	250	0.71	1,000	12	0	16.4	4.7	3.37E-10	29.8	-45
4	411	197	182	250	0.70	300	12	3,600	16.6	0.0	2.55E-10	29.5	-44
5	479	203	188	250	0.70	300	12	9,700	16.7	0.0	1.74E-10	29.4	-43
6	605	175	185	250	0.70	300	12	9,700	18.7	0.0	2.78E-10	29.1	-36
7	746	-526	-258	<30	0.70	300	12	9,700	19.3	0.0	5.73E-11	29.0	-33

[a]Laboratory–prepared Type 304 SS (Heat 10285) SMA weld HAZ, irradiated to 5.0 x 10^{20} n cm^{-2}.
[b]An asterisk indicates environmental enhancement of growth rates under cyclic loading.
[c]Represents values in the effluent. Conductivity was ≈0.07 and 0.2 µS/cm in feedwater and effluent, respectively.
[d]Based on flow stress.

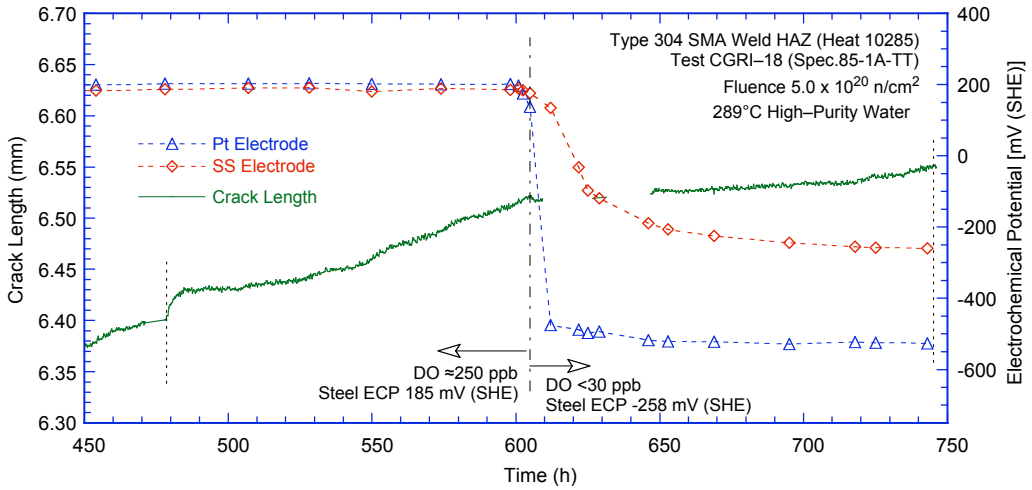

Figure 36. Change in crack length and ECP of Pt and SS electrodes when the DO level in feedwater was decreased from ≈250 to <30 ppb.

After the J–R curve test, the final crack front was marked by fatigue cycling at room temperature in air. The specimen was then fractured, and the fracture surface of both halves of the specimen was photographed with a telephoto lens through the cell window, Fig. 37. The final crack length was measured from the photograph by the 9/8 averaging technique; the difference in measured and estimated crack lengths was <5%. The crack extensions estimated from the DC potential drop method were 0.71 and 0.82 mm for the CGR and J–R curve test portions, respectively.

The fracture surface was also examined by SEM to verify the crack extensions during CGR and J–R tests and to characterize the fracture morphology. A micrograph of the entire crack extension, i.e., for both CGR and J–R curve test, is shown in Fig. 38. Once again, a relatively straight crack front is observed. Measurements of the final crack length show very good agreement with the values estimated from the DC potential drop method and those measured earlier from photographs of the fracture surface; the difference in measured and estimated crack lengths was <5%.

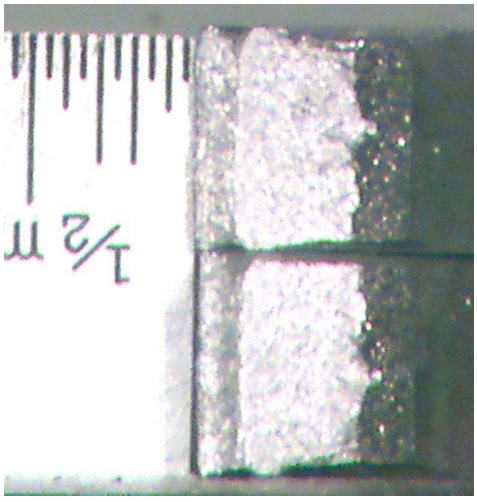

Figure 37. Photomicrograph of the fracture surface of Specimen 85-1A TT.

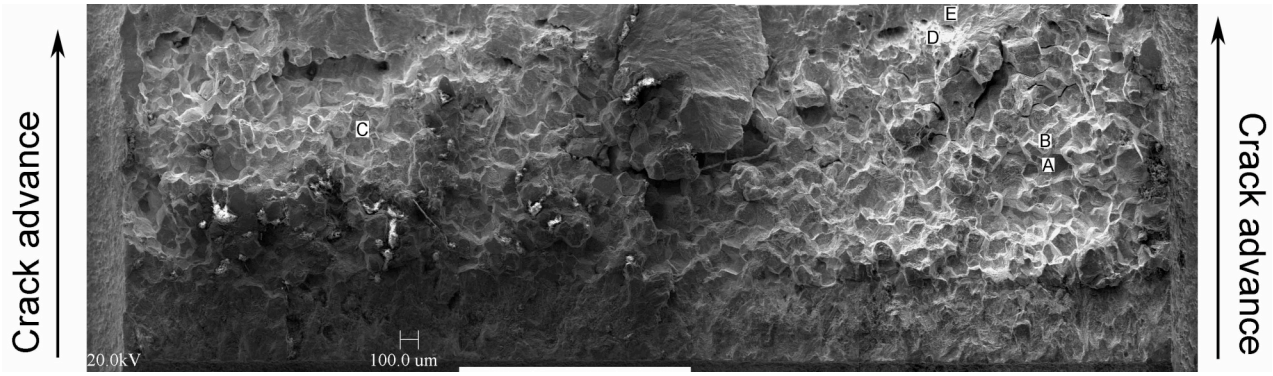

Figure 38. Micrograph of the fracture surface of Specimen 85-1A-TT tested in BWR environments.

The changes in crack length and K_{max} with time during various test periods are shown in Fig. 39. In general, the DC potential measurements show very little scatter; the fluctuations in K_{max} at 400–600 h were caused by changes in the system pressure. For this specimen, environmental enhancement occurred after ≈190 h during test period 1b, Fig. 39a. Also, the results in Table 9 indicate that for this specimen, the applied K_{max} during all test periods was within the values allowed by the K/size criterion of Eq. 13.

A significant feature of the fracture surface is the essentially intergranular (IG) nature of the fracture during the J–R curve test in high–DO water, in contrast to the ductile fracture morphology expected in a J–R test in air. High magnification micrographs at locations A–E in Fig. 38 are shown in Figs. 40–42. All these locations correspond to the portion of the fracture surface associated with the J–R curve test. All except location E, which is near the end of the test, show predominantly IG fracture. Some facets show an increased degree of deformation (e.g., Fig. 40), and occasional TG areas occur with stepped or terrace–like fracture planes.

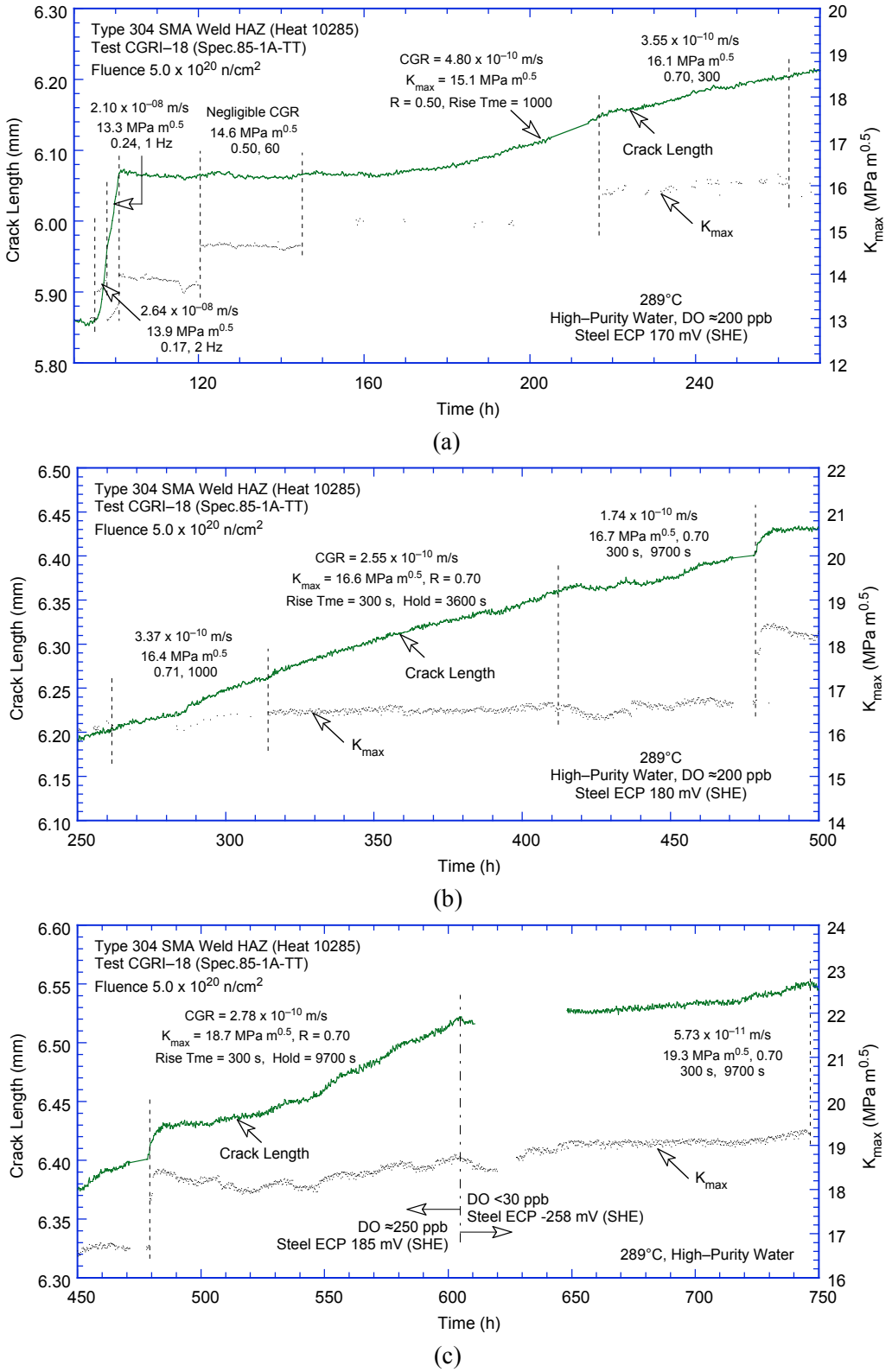

Figure 39. Crack–length–vs.–time plots for irradiated SMA weld HAZ Specimen 85-1A-TT in high-purity water at 289°C during test periods (a) 1–2, (b) 3–5, and (c) 6–7.

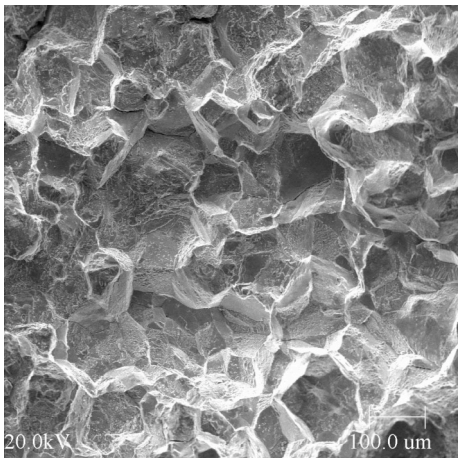

a

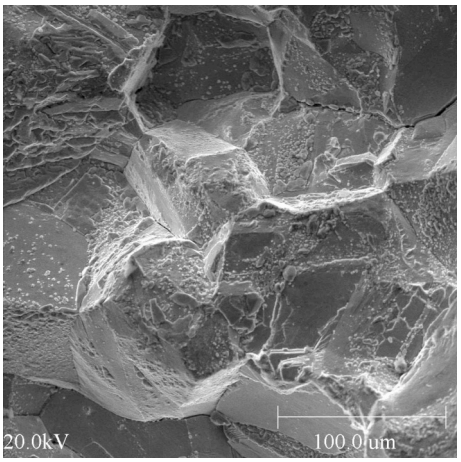

b

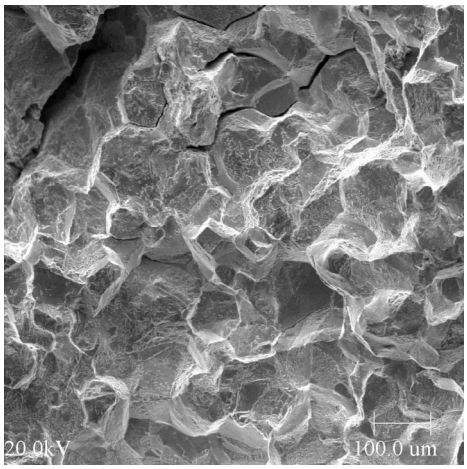

c

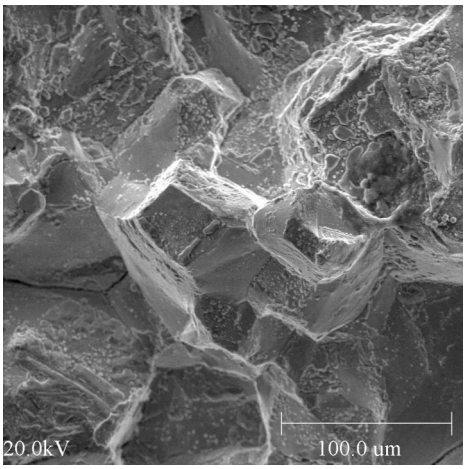

d

Figure 40. Micrographs showing the fracture surface of 85-1A-TT at positions A and B in Fig. 38. Figures b and d are high magnification of a and c.

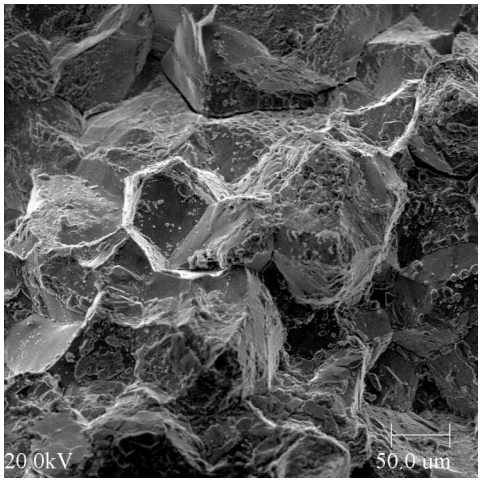

a

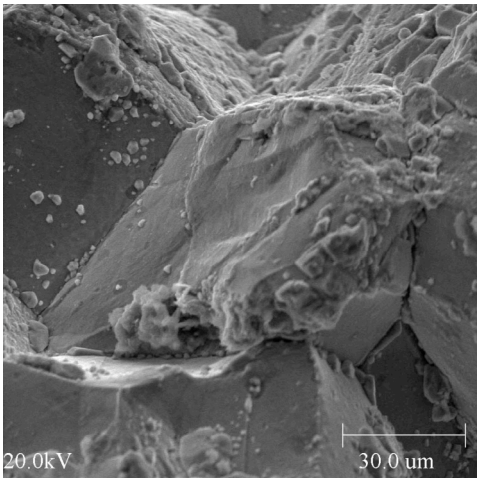

b

Figure 41. Micrographs showing the fracture surface of 85-1A-TT at position C in Fig. 38. Figure b is high magnification of a.

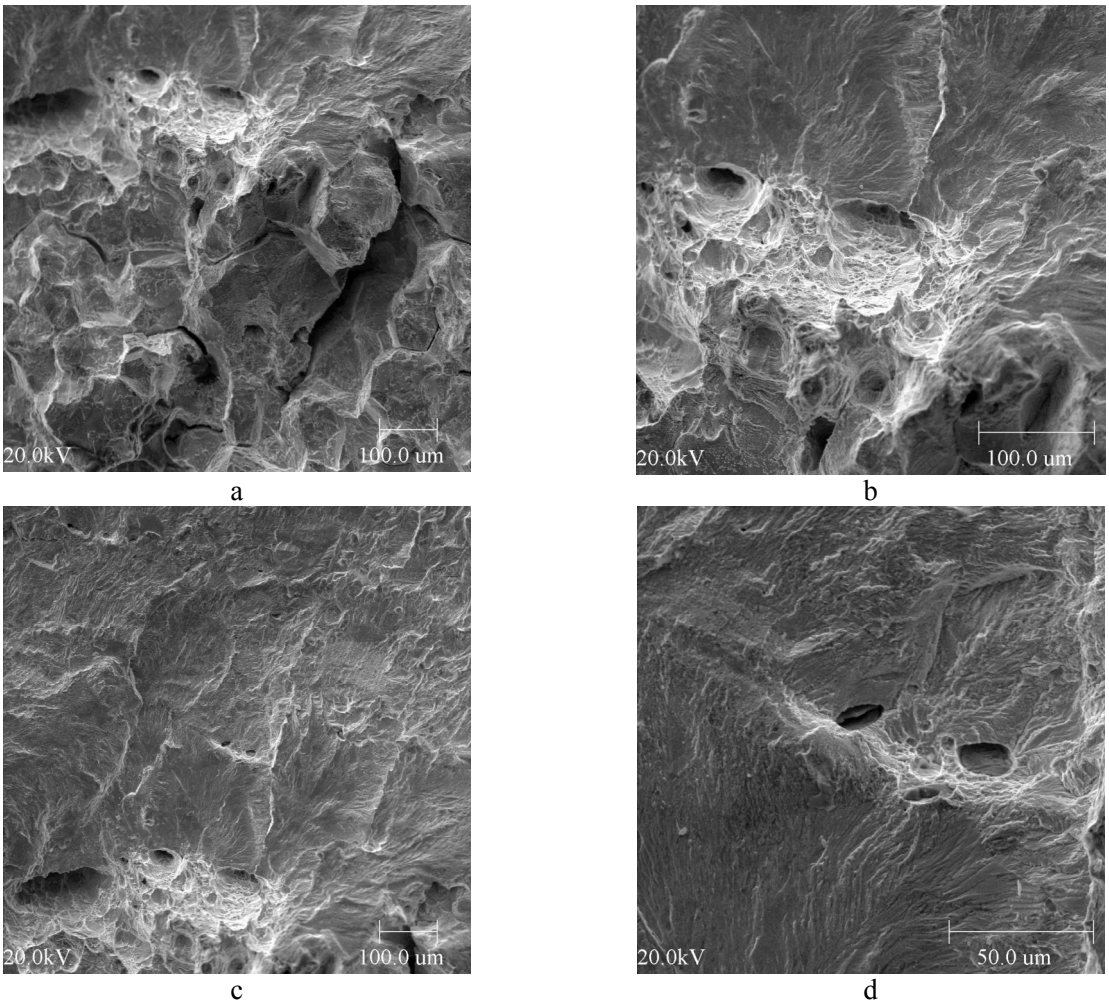

Figure 42. Micrographs showing the fracture surface of 85-1A-TT at positions D and E in Fig. 38. Figures b and d are high magnification of a and c.

A section of the entire crack extension is shown in Fig. 43a, and high–magnification micrographs of select locations of the fracture surface, designated A–D in Fig. 43a, are shown in Figs. 43b–e. A measurement bar is also included in Fig. 43a to help define the approximate position of the crack front after the various test periods. The micrographs of locations A–C in Figs. 43b–d are from the CGR test region, and location D in Fig. 43e is from the J–R curve test. For the CGR test, the fracture morphology is TG initially and changes to IG beyond ≈0.27 mm, Fig. 43a. These results show good agreement with the measured CGRs; an environmental enhancement of growth rates occurred after ≈0.26–mm crack extension.

The experimental results from the J–R curve test were analyzed in accordance with ASTM E-1737 to obtain the fracture toughness J–R curve for Specimen 85–1A–TT in BWR water. The displacement of load pins was determined by subtracting the extension of the load train from the measured extension. The load train extension was determined as a function of applied load using a very stiff specimen. The blunting line was defined by the relationship $\Delta a = J/(4\sigma_f)$, where σ_f is the effective flow stress defined as the average of the nonirradiated and irradiated flow stress.

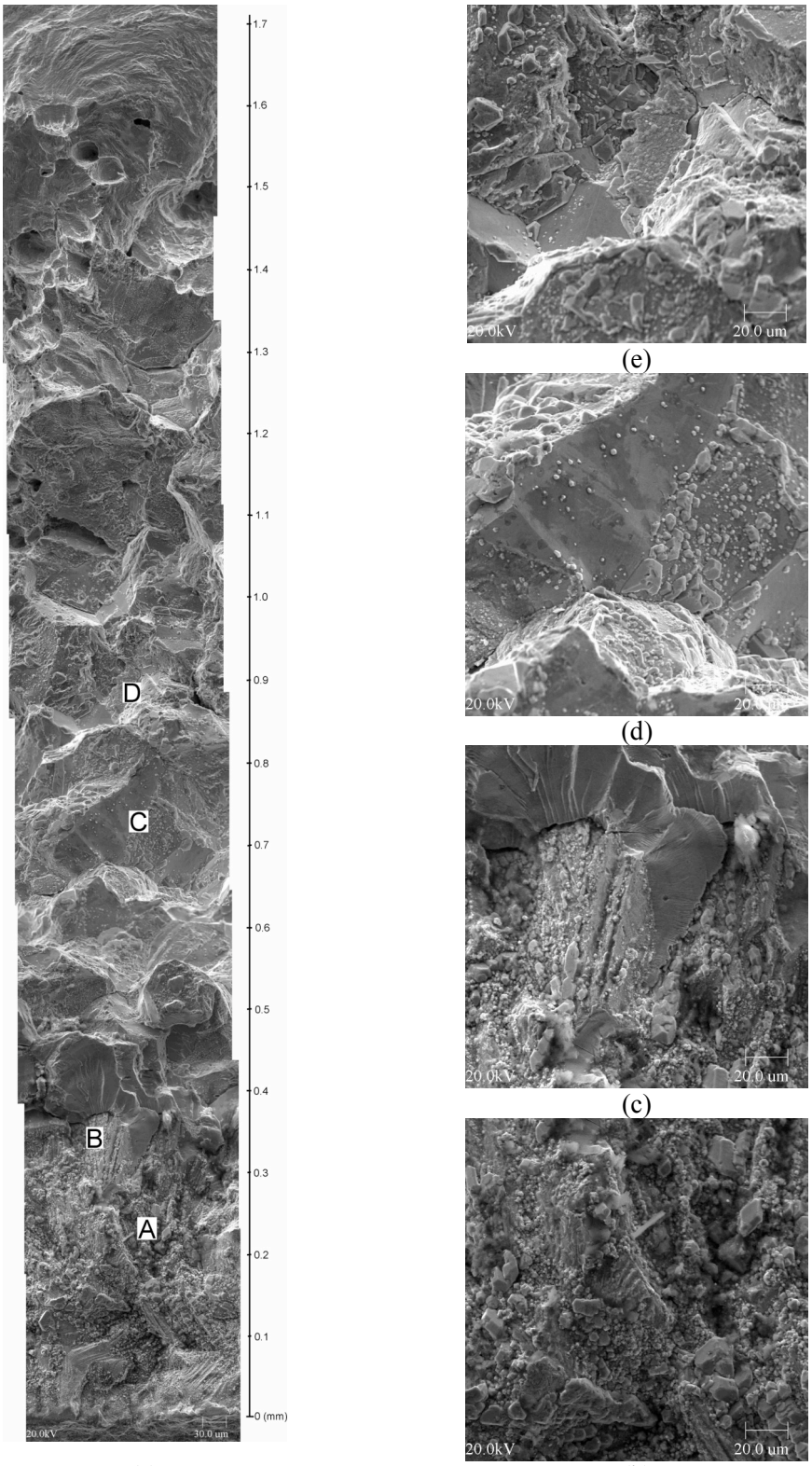

Figure 43. Photomicrographs showing (a) a slice of the entire length of the fracture surface and (b), (c), (d), and (e) high–magnification photomicrographs of the fracture surface at positions A, B, C, and D, respectively.

The load–vs.–load-line displacement curve and the fracture toughness J–R curve for the Specimen 85–1A–TT is shown in Figs. 44 and 45, respectively. The results yield a J_{Ic} value of ≈345 kJ/m^2 for the material. This value is lower than those observed earlier[19] for other heats of austenitic SS in air; the J_{Ic} values were 368 and 378 kJ/m^2, respectively, for Type 304 and Type 316L SS irradiated to 0.9 x 10^{21} n/cm^2.

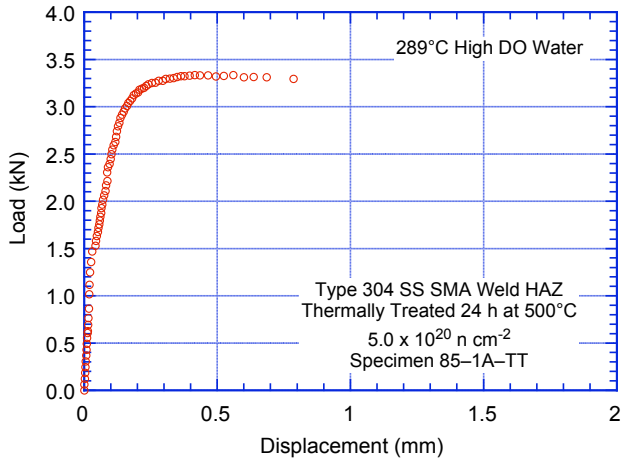

Figure 44.
Load vs. load-line displacement curve for irradiated SMA weld HAZ Specimen 85-1A-TT in high-purity water at 289°C.

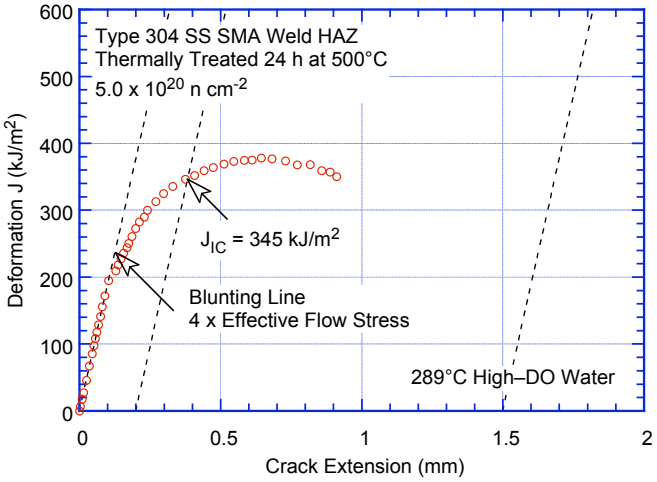

Figure 45.
Fracture toughness J–R curve for irradiated SMA weld HAZ Specimen 85-1A-TT in high-purity water at 289°C.

3.2.4 Specimen 85–7A of Type 304 SS HAZ Irradiated to 5.0 x 10^{20} n/cm^2

The test conditions, experimental CGRs, the allowed K_{max} from K/size criterion, and the margin between the applied and allowed values of K_{max} are given in Table 10 for Specimen 85–7A. The test was started in high–purity water with ≈500 ppb DO and ≈10.0 mL/min flow rate. The ECP of a Pt electrode and a SS sample located at the exit of the autoclave were monitored continuously during the test, while the water DO and conductivity were determined periodically. Precracking was carried out at R = 0.2, K_{max} = 15.5 MPa m$^{1/2}$, and triangular waveform with 1 Hz frequency. The crack grew ≈0.1 mm in the precracking phase. The R ratio was increased to 0.5, and the rise time increased to 60–1000 s to begin the transition from TG fatigue crack growth to IG SCC growth. The changes in crack length and K_{max} with time during various test periods are shown in Fig. 46. For this specimen, significant environmental enhancement of growth rates occurred during test period 5, Fig. 46b.

Table 10. Crack growth data for specimen 85–7A of SS SMA Weld HAZ in high–purity water[a] at 289°C.

Test Period[b]	Test Time, h	ECP,[c] mV (SHE) Pt	ECP,[c] mV (SHE) Steel	O_2 Conc.,[c] ppb	R Load Ratio	Rise Time, s	Down Time, s	Hold Time, s	K_{max}, MPa·m$^{1/2}$	ΔK, MPa·m$^{1/2}$	Growth Rate, m/s	Allowed K_{max}, MPa·m$^{1/2}$	Margin in K_{max},[d] %
Pre	166	261	224	500	0.23	0.5	0.5	0	15.9	12.2	2.77E-08	29.7	-47
1	187	258	225	500	0.50	60	4	0	15.8	7.9	negligible	29.7	-47
2	428	244	219	500	0.51	300	4	0	15.7	7.7	2.09E-11	29.6	-47
3	499	245	221	500	0.50	1000	12	0	16.3	8.2	negligible	29.6	-45
4	608	234	211	500	0.53	1000	12	0	17.2	8.1	4.65e-11	29.6	-42
5*	763	229	209	500	0.50	1000	12	0	18.3	9.1	4.28e-10	29.1	-37
6*	788	231	212	500	0.50	1000	12	3600	18.6	9.3	9.51e-10	28.8	-36
7	845	221	214	500	1.00	-	-	-	19.4	-	9.46e-10	28.3	-32
8	1100	-527	-252	<50	1.00	-	-	-	19.8	-	1.55E-11	28.0	-29

[a]Laboratory–prepared SMA weld HAZ, irradiated to 0.5 x 10^{21} n cm^{-2}.
[b]An asterisk indicates environmental enhancement of growth rates under cyclic loading.
[c]Represents values in the effluent. Conductivity was ≈0.07 and 0.3 µS/cm in feedwater and effluent, respectively.
[d]Based on flow stress.

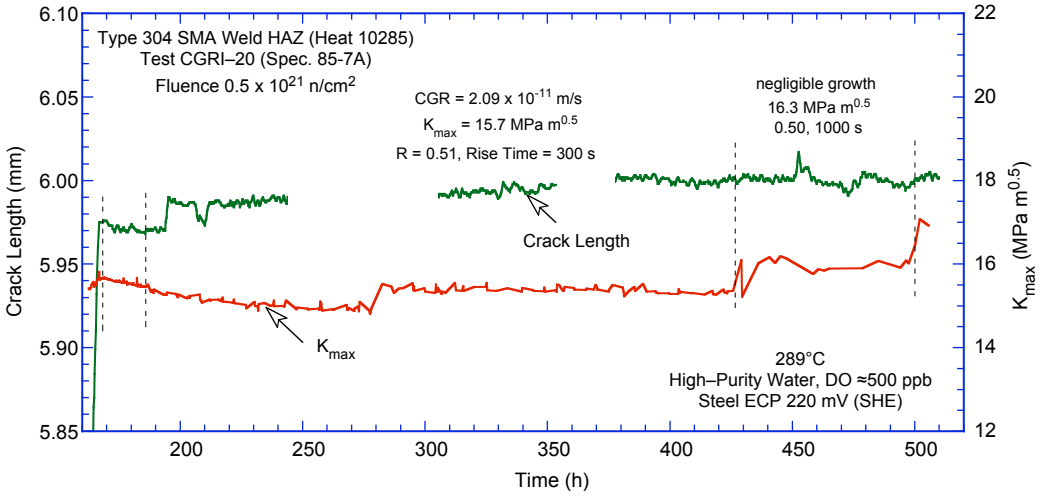

(a)

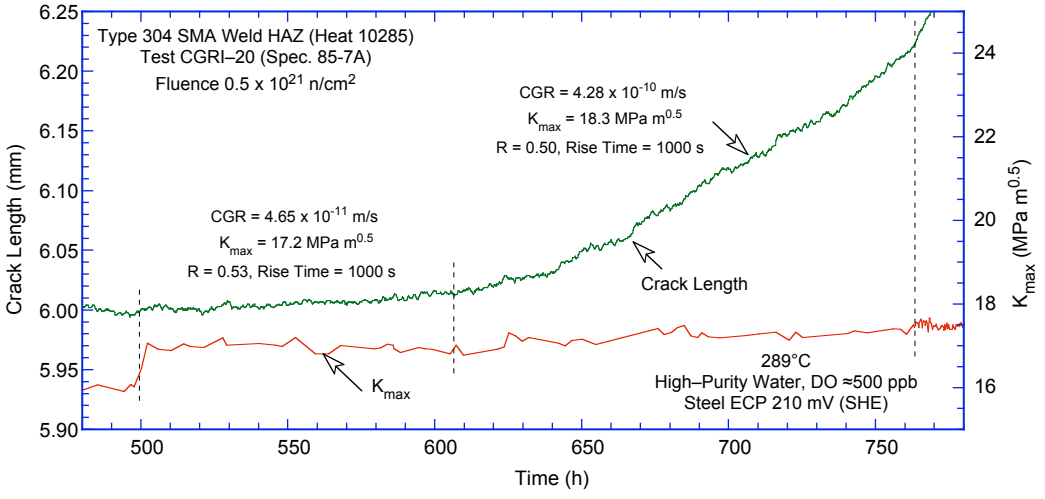

(b)

Figure 46. Crack–length–vs.–time plots for irradiated SMA weld HAZ Specimen 85-7A in high-purity water at 289°C during test periods (a) 1–3, (b) 4–5 and (c) 6–8.

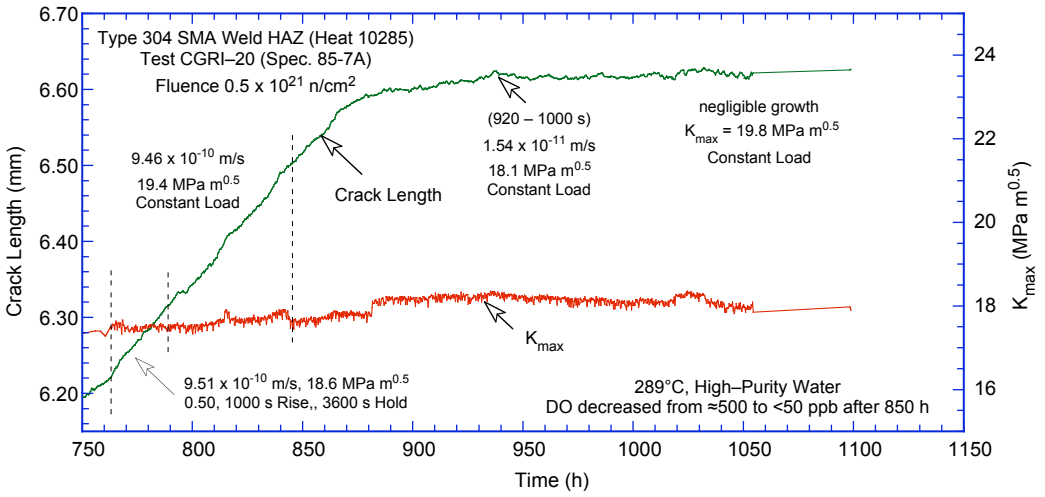

(c)

Figure 46. (Contd.)

After the CGR test, the final crack front was marked by fatigue cycling at room temperature in air. The specimen was then fractured, and the fracture surfaces of both halves of the specimen were photographed with a telephoto lens through the cell window, Fig. 47. The actual crack extension was ≈80% greater than the value determined from the DC potential measurements. Crack extensions estimated from the DC potential drop method were scaled proportionately; the corrected values of K_{max} and growth rates are listed in Table 10. For this specimen, loading conditions for the entire test satisfy the K/size criterion of Eq. 13.

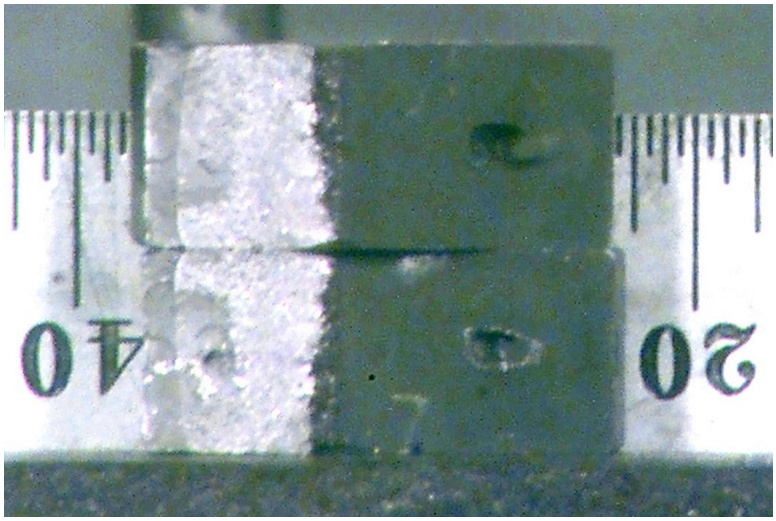

Figure 47. Photomicrograph of the fracture surface of Specimen 85-7A.

3.2.5 CGRs of Austenitic SS Weld HAZ under Continuous Cycling

For continuous cyclic loading, the experimental CGRs for irradiated and nonirradiated SS weld HAZ specimens in high–DO environment and those predicted in air for the same loading conditions are plotted in Fig. 48. The curves represent the Shack/Kassner model for nonirradiated austenitic SSs in high–purity water with 8 ppm DO (Eq. 11) and are included to provide a comparison with the irradiated

CGR data. The CGRs in air, $\dot{a}_{air}$ (m/s), were determined from the correlations developed by James and Jones[29] (Eqs. 7–9). In Fig. 48b, although the loading conditions for the data points shown with a "+" did not satisfy the K/size criterion of Eq. 13, they were only ≈10% higher than those allowed by the criterion of Eq. 14. The K/size criterion of Eq. 14 may be acceptable under cyclic loading.

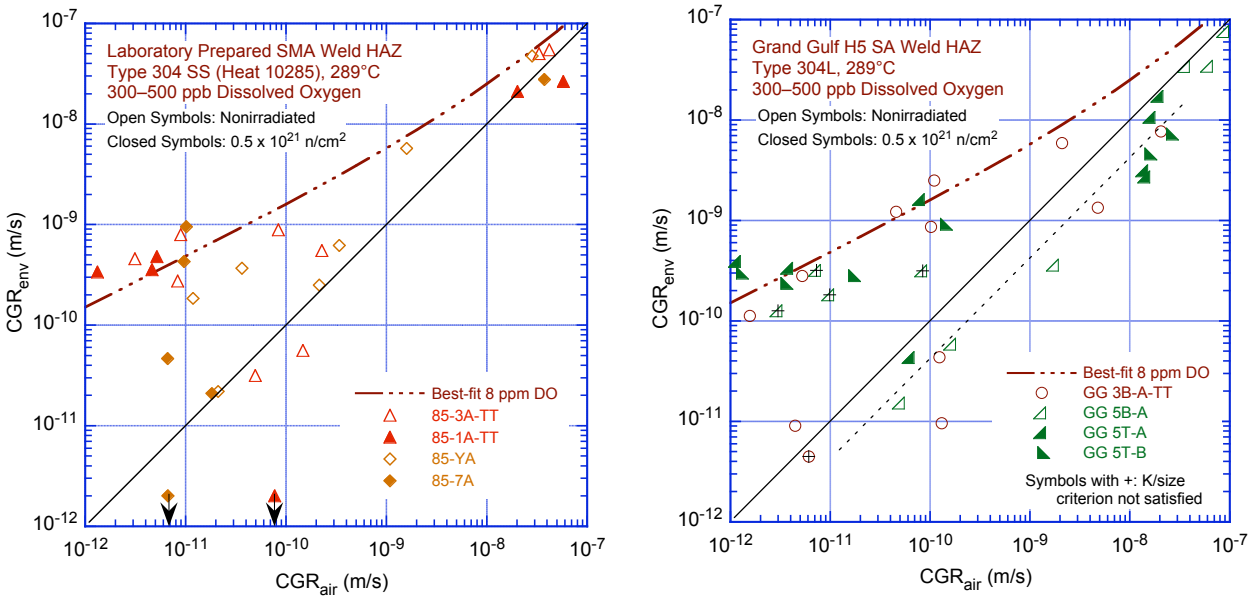

(a) (b)

Figure 48. CGR data for irradiated and nonirradiated specimens of (a) laboratory–prepared Type 304 SS SMA weld HAZ and (b) Type 304L SA weld HAZ from the Grand Gulf core shroud under continuous cycling at 289°C in high–purity water with 300–500 ppb dissolved oxygen.

In these figures, the data points that lie along the diagonal represent predominantly mechanical fatigue and those that lie close to the Shack/Kassner model indicate environmentally enhanced crack growth. For both irradiated and nonirradiated specimens, enhancement of CGR did not occur readily as depicted in Fig. 12 when the load ratio and rise time were increased. For example, a large number of data points lie along the diagonal in Fig. 48, particularly for the GG Type 304L weld HAZ. The applied K_{max} had to be increased for enhanced growth rates.

The results indicate that under mechanical fatigue loading (i.e., no environmental enhancement), the CGRs for the GG Type 304L SA weld HAZ are lower than those for the Type 304 SMA weld HAZ, e.g., the CGRs for laboratory–prepared Type 304 weld HAZ (Fig. 48a) show good agreement with those predicted by Eqs. 7–9 where as those for the GG weld HAZ are a factor of ≈2 lower (dashed line in Fig. 48b). Also, under this type of loading thermal treatment of the material for 24 h at 500°C or irradiation to 5.0 x 10^{20} n/cm^2 (E > 1 MeV) (≈0.75 dpa) has little or no effect on growth rates.

In the high–DO NWC BWR environment (under environmentally enhanced condition), the CGRs of the laboratory–prepared Type 304 SS SMA weld HAZ (Fig. 48a) and those of the GG Type 304L SA weld HAZ (Fig. 48b) are comparable. For nonirradiated material of either GG or laboratory–prepared weld HAZ, the growth rates of the as–welded plus thermally–treated condition (open triangles in Fig. 48a and open circles in Fig. 48b) are marginally higher than those of the as–welded condition (open diamonds in Fig. 48a and open right–angle triangles in Fig. 48b). The results for nonirradiated GG weld HAZ are in good agreement with the data obtained by Andresen et al.[26] for GG Type 304L weld HAZ in high–DO

water (2000 ppb DO) at 288°C. For example, Andresen obtained a CGR of 3.4 x 10^{-10} m/s at R = 0.7, K_{max} = 27.4 MPa $m^{1/2}$, and triangular waveform with 500 s rise time.

For both the GG and laboratory–prepared weld HAZs, irradiation to ≈0.75 dpa has little or no effect on growth rates of the thermally–treated material, whereas the growth rates of as–welded material are increased such that they are comparable to those of the thermally–treated material. In high–DO NWC BWR water, the CGRs for irradiated and nonirradiated thermally–treated HAZ and irradiated as–welded HAZ may be represented by the Shack/Kassner model for nonirradiated austenitic SSs in high–purity water with 8 ppm DO; the rates for nonirradiated as–welded HAZ are slightly lower.

Metallographic examination of the fractured specimens indicates that under environmentally enhanced growth conditions (i.e., the data points that lie close to the Shack/Kassner model), an IG fracture morphology is observed for both the irradiated and nonirradiated laboratory–prepared Type 304 SS weld HAZ (Figs. 22 and 38). Transgranular fracture morphology is observed under conditions that show little or no environmental enhancement (i.e., data points that lie close to the diagonal in Fig. 48a) and are predominantly due to mechanical fatigue. Although metallographic examination of the irradiated GG Type 304L HAZ has not been completed, the results for the nonirradiated material indicate that the fracture morphology of GG Type 304L HAZ is different from that for Type 304 SMA weld HAZ. For example, in the GG Type 304L HAZ, a TG fracture morphology with a well–defined river pattern is observed under all loading conditions, even where growth is environmentally enhanced (Figs. 16 and 26). IG fracture morphologies are usually observed in cold–worked SSs, whether initially annealed or sensitized.[24,26,27] Because of the residual strain associated with the welding process, the observed TG fracture morphology would not be expected in SS weld HAZ, especially for a case in which the environment enhancement is substantial. The reasons for this unexpected behavior are unclear.

3.2.6 CGRs of Austenitic SS Weld HAZ under Constant Load or Cycling with Long Hold Periods

For CGR tests under constant load or a trapezoidal waveform with long hold periods (i.e., constant load with periodic partial unloading), the experimental CGRs for nonirradiated and irradiated SS weld HAZ specimens in high–DO environment are shown in Figs. 49a and b, respectively. Although three materials were tested with and without irradiation, SCC growth rates for both nonirradiated and irradiated conditions were obtained for two materials only, e.g., as–welded GG Type 304L weld HAZ (right angle triangles in Fig. 49) and as–welded plus thermally–treated Type 304 weld HAZ (triangles in Fig. 49). Crack growth rate data were not obtained for the nonirradiated, as–welded laboratory–prepared Type 304 weld HAZ. Also, as discussed in Section 3.1.3, the three very low values of growth rate (<1 x 10^{-11} m/s) observed for Specimen GG3B–A–TT (Table 5) were most likely influenced by the accidental overstrain of the specimen and, therefore, are excluded from the figure.

For nonirradiated GG Type 304L weld HAZ, the as–welded (right angle triangles in Fig. 49a) and as–welded plus thermally–treated (circles in Fig. 49a) materials have comparable CGRs. For both conditions, the CGRs are a factor of ≈2 lower than the NUREG–0313 curve for sensitized SSs in water with 8 ppm DO. The results for the nonirradiated GG weld HAZ are in agreement with the CGR of 1 x 10^{-10} m/s for GG Type 304L weld HAZ at K_{max} = 27.4 MPa $m^{1/2}$ in high–DO water (2000 ppb DO) at 288°C obtained by Andresen et al.[26]. The CGR for nonirradiated thermally–treated Type 304 SS weld HAZ (open triangle in Fig. 49a) is a factor of ≈10 higher than the CGRs for Type 304L weld HAZ; the rates for as–welded Type 304 SS weld HAZ were not obtained. The CGR of the thermally–treated Type 304 SS weld HAZ is a factor of ≈5 higher than the NUREG–0313 curve.

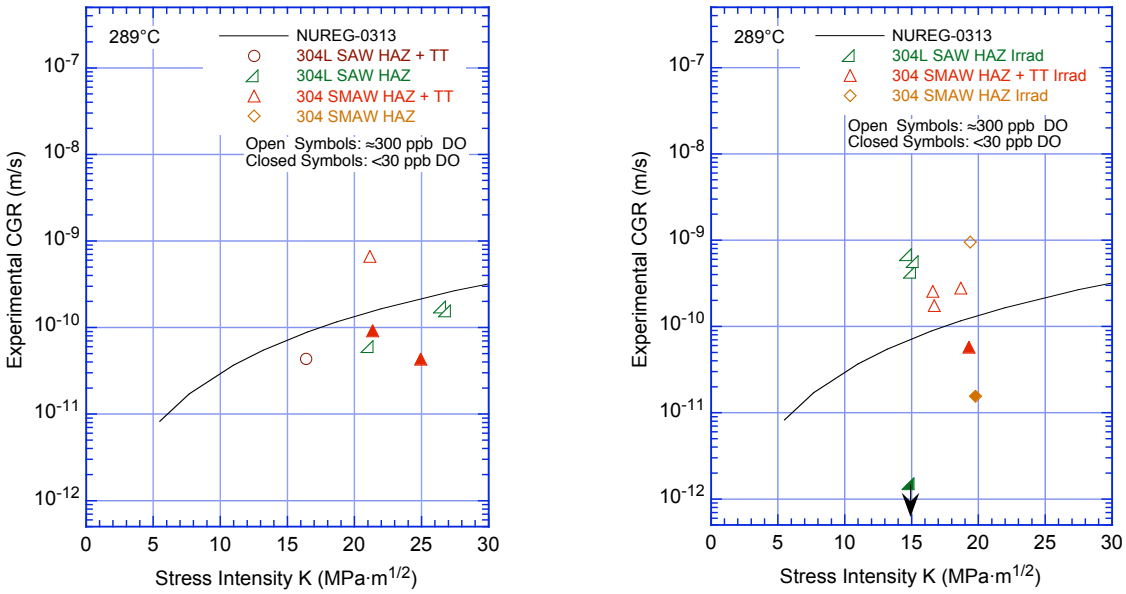

(a) (b)

Figure 49. CGR data under constant load with periodic partial unloads for (a) nonirradiated and (b) irradiated SS weld HAZ specimens in high–purity water at 289°C.

The fracture morphology of the two materials is also different, e.g., TG for the Type 304L SA weld HAZ and IG for the Type 304 SMA weld HAZ. As discussed in the last section, a TG morphology is unusual in SS weld HAZ, e.g., the presence of residual strain in the material typically promote IG crack growth even in nonsensitized SS.[24,26,27] An IG fracture is observed in all cold–worked SSs. Additional tests will be conducted on the nonirradiated GG Type 304L weld HAZ material to establish its fracture behavior.

The CGRs of all the SS weld HAZ materials irradiated to 5.0 x 10^{20} n/cm^2 (≈0.75 dpa) are a factor of 2–5 higher than the NUREG–0313 disposition curve for sensitized SSs in high–DO water. Irradiation increased the CGRs of as–welded Type 304L weld HAZ (right angle triangle in Fig. 49b), whereas it had little or no effect on the CGRs of as–welded plus heat–treated Type 304 weld HAZ (triangles in Fig. 49b). For the latter, the experimental CGRs of the irradiated material are, in fact, lower than the rate of nonirradiated material. The fracture morphology for irradiated Type 304 weld HAZ is similar to the nonirradiated material, e.g., fracture morphology is IG under environmentally enhanced growth conditions or SCC conditions, and TG under mechanical fatigue or conditions that show little or no environmental enhancement.

A beneficial effect of reducing the corrosion potential of the environment was observed for all materials that were tested in BWR environment. The growth rates of irradiated or nonirradiated Type 304 weld HAZ decreased by a factor of ≈8, and those for irradiated Type 304L weld HAZ decreased by nearly two orders of magnitude when the DO was decreased from ≈300 ppb to <30 ppb.

For the irradiated materials, the SCC growth rates under constant or long-hold time trapezoidal loads are comparable to the growth rates observed under cyclic loading corresponding to CGRs in air < 10^{-11} m/s. For the nonirradiated materials, the SCC growth rates under constant or long-hold time trapezoidal loads are a factor of 2-4 lower than the growth rates observed under cyclic loading

corresponding to CGRs in air < 10^{-11} m/s. Under cyclic loading, there was little difference in the CGRs of the irradiated and nonirradiated materials, this was not the case under constant load.

3.2.7 Fracture Toughness of Irradiated Austenitic SS Weld HAZ in High-Purity Water at 288°C

The fracture toughness J–R curve was determined for irradiated Type 304 SS SMA weld HAZ (Specimen 85–1A–TT) in high–DO water at 288°C. The experimental J_{Ic} for this material and those obtained earlier[19] for two commercial heats (C19 and C16) in air are plotted as a function of neutron exposure in Fig. 50. Results of tests on Type 304 SS reactor internal materials from operating BWRs[2] are also included in the figure. The fracture toughness J_{Ic} in high–DO water is slightly lower than that in air. Also, a significant result for the J–R curve test in high–DO water is the essentially IG fracture morphology (Fig. 40 and 41) as opposed to the ductile fracture morphology expected in a test in air.

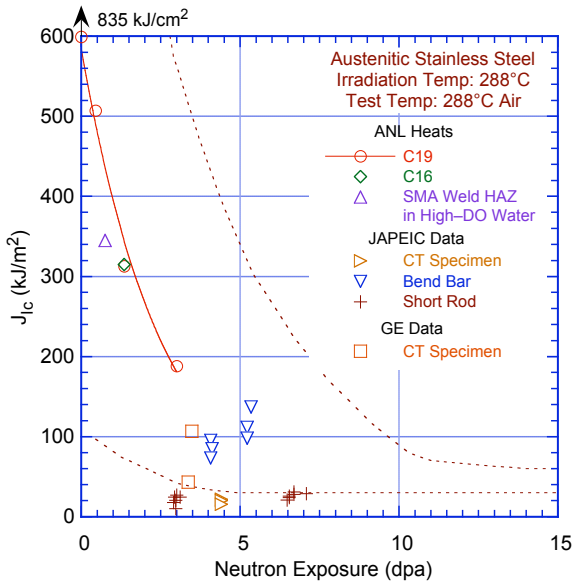

Figure 50.
Fracture toughness J_{Ic} as a function of neutron exposure at 288°C for austenitic SSs in air and SS SMA weld HAZ in high–purity water. Dashed lines represent upper and lower bounds for change in J_{Ic} for austenitic SSs irradiated at 350–450°C.
JAPEIC = Japan Power Engineering and Inspection Corporation, GE = General Electric Nuclear Energy.

4. Summary

Crack growth rate tests have been conducted on austenitic SS weld HAZ specimens that were irradiated to 5 x 10^{20} n/cm^2 (E > 1 MeV) (≈0.75 dpa) at ≈288°C in a helium environment in the Halden boiling heavy water reactor. The tests were conducted on 1/4–T CT specimens in NWC (300–500 ppb DO) and HWC (≤50 ppb DO) BWR environments under cyclic loading with a slow/fast sawtooth waveform or a trapezoidal waveform with long hold periods. The latter essentially represents constant load with periodic partial unloads. Crack extensions were monitored by DC potential drop measurements.

The specimens were obtained from Type 304L SS HAZ of the H5 SA weld of the GG reactor core shroud and Type 304 SS HAZ of a laboratory–prepared SMA weld. The materials were tested in two conditions: as–welded and as–welded plus thermally treated for 24 h at 500°C. Baseline data were obtained on nonirradiated specimens. Specimen irradiations were performed in the Halden test reactor in Norway.

The significant results for the cyclic growth rates are as follows:

(a) Under loading conditions that resulted in predominantly mechanical fatigue (i.e., no environmental enhancement), experimental CGRs for the GG Type 304L weld HAZ are lower than those for the Type 304 SMA weld HAZ. The CGRs for Type 304 weld HAZ are consistent, and those for the GG weld HAZ are a factor of ≈2 lower than those predicted for austenitic SSs in air. Also, thermal treatment of the material for 24 h at 500°C to simulate low–temperature sensitization has little or no effect on mechanical fatigue growth rates.

(b) In the high–DO NWC BWR environment at 289°C (i.e., with environmental enhancement), the cyclic CGRs of Type 304 SS SMA weld HAZ are comparable to those of the GG Type 304L SA weld HAZ. For nonirradiated material of either the GG or the laboratory–prepared weld HAZ, the growth rates of the thermally–treated condition are marginally higher than those of the as–welded condition.

(c) For both the GG and the laboratory–prepared weld HAZ, irradiation to ≈0.75 dpa has little or no effect on the cyclic CGRs of the thermally–treated material, whereas the CGRs of as–welded material are increased such that they are comparable to those of the thermally–treated material.

(d) For the Type 304 SS weld HAZ, IG fracture is observed under conditions that show environmental enhancement of growth rates. A TG fracture is observed under conditions that show little or no environmental enhancement and predominantly mechanical fatigue. Although metallographic examination of the irradiated Type 304L HAZ has not been completed, the results for the nonirradiated material indicate a TG fracture with well–defined river pattern under all loading conditions, even under environmentally enhanced growth conditions.

The SCC growth rates are somewhat different from the growth rates under cyclic loading. The significant results for the SCC growth rates are as follows:

(a) For nonirradiated GG Type 304L weld HAZ, the CGRs of as–welded and as–welded plus thermally–treated material are comparable. For both conditions, the CGRs are a factor of ≈2 lower than the NUREG–0313 curve for sensitized SSs in water with 8 ppm DO.

(b) For the nonirradiated thermally–treated Type 304 SS weld HAZ, the CGR is a factor of ≈10 higher than the CGRs for the Type 304L weld HAZ, and the rate is a factor of ≈5 higher than the NUREG–0313 curve. Crack growth rates for the as–welded Type 304 SS weld HAZ were not obtained.

(c) The CGRs of all the SS weld HAZ materials irradiated to 5.0×10^{20} n/cm^2 (≈0.75 dpa) are a factor of 2–5 higher than the NUREG–0313 disposition curve for sensitized SSs in high–DO water. Irradiation increased the CGRs of as–welded Type 304L weld HAZ, whereas it had little or no effect on the CGRs of the as–welded plus heat–treated Type 304 weld HAZ.

(d) The fracture morphology for the irradiated Type 304 weld HAZ is similar to the nonirradiated material: the fracture morphology is IG under environmentally enhanced growth conditions or SCC conditions, and TG under mechanical fatigue or conditions that show little or no environmental enhancement.

(e) A beneficial effect of reducing the corrosion potential of the environment on growth rates was observed for all materials that were tested in BWR environment. The growth rates of irradiated or nonirradiated Type 304 weld HAZ decreased by a factor of ≈8, and those for irradiated Type 304L weld HAZ decreased by nearly two orders of magnitude when the DO was decreased from ≈300 ppb to <30 ppb.

References

1. Bruemmer, S. M., et al., "Critical Issue Reviews for the Understanding and Evaluation of Irradiation–Assisted Stress Corrosion Cracking," EPRI TR–107159, Electric Power Research Institute, Palo Alto, CA, 1996.

2. Herrera, M. L., et al., "Evaluation of the Effects of Irradiation on the Fracture Toughness of BWR Internal Components," in Proc. ASME/JSME 4th Intl. Conf. on Nucl. Eng. (ICONE–4) Vol. 5, A. S. Rao, R. M. Duffey, and D. Elias, eds., American Society of Mechanical Engineers, New York, pp. 245–251, 1996.

3. Mills, W. J., "Fracture Toughness of Type 304 and 316 Stainless Steels and their Welds," Intl. Mater. Rev. 42, 45–82, 1997.

4. Kanasaki, H., I. Satoh, M. Koyama, T. Okubo, T. R. Mager, and R. G. Lott, "Fatigue and Stress Corrosion Cracking Behaviors of Irradiated Stainless Steels in PWR Primary Water," Proc. 5th Intl. Conf. on Nuclear Engineering, ICONE 5-2372, pp. 1–7, 1997.

5. Andresen, P. L., F. P. Ford, S. M. Murphy, and J. M. Perks, "State of Knowledge of Radiation Effects on Environmental Cracking in Light Water Reactor Core Materials," Proc. 4th Intl. Symp. on Environmental Degradation of Materials in Nuclear Power Systems – Water Reactors, NACE, pp. 1.83–1.121, 1990.

6. Jenssen, A., and L. G. Ljungberg, "Irradiation Assisted Stress Corrosion Cracking of Stainless Alloys in BWR Normal Water Chemistry and Hydrogen Water Chemistry," Proc. Sixth Intl. Symp. on Environmental Degradation of Materials in Nuclear Power Systems – Water Reactor, R. E. Gold and E. P. Simonen, eds., Minerals, Metals & Materials Society, pp. 547–553, 1993.

7. Brown, K. S., and G. M. Gordon, "Effects of BWR Coolant Chemistry on the Propensity for IGSCC Initiation and Growth in Creviced Reactor Internals Components," Proc. Third Intl. Symp. on Environmental Degradation of Materials in Nuclear Power Systems – Water Reactor, The Metallurgical Society, Warrendale, PA, pp. 243–248, 1987.

8. Gordon, G. M., and K. S. Brown, "Dependence of Creviced BWR Component IGSCC Behavior on Coolant Chemistry," Proc. 4th Intl. Symp. on Environmental Degradation of Materials in Nuclear Power Systems – Water Reactor, Daniel Cubicciotti, ed., NACE, pp. 14.46–14.61, 1990.

9. Garzarolli, F., D. Alter, and P. Dewes, "Deformability of Austenitic Stainless Steels and Nickel–Base Alloys in the Core of a Boiling and a Pressurized Water Reactor," Proc. Intl. Symp. on Environmental Degradation of Materials in Nuclear Power Systems – Water Reactor, ANS, pp. 131–138, 1986.

10. Kodama, M., et al., "IASCC Susceptibility of Austenitic Stainless Steels Irradiated to High Neutron Fluence," Proc. Sixth Intl. Symp. on Environmental Degradation of Materials in Nuclear Power Systems – Water Reactor, R. E. Gold and E. P. Simonen, eds., Minerals, Metals & Materials Society, pp. 583–588, 1993.

11. Kodama, M., et al., "Effects of Fluence and Dissolved Oxygen on IASCC in Austenitic Stainless Steels," Proc. Fifth Intl. Symp. on Environmental Degradation of Materials in Nuclear Power Systems – Water Reactor, American Nuclear Society, pp. 948–954, 1991.

12. Clark, W. L., and A. J. Jacobs, "Effect of Radiation Environment on SCC of Austenitic Materials," Proc. First Intl. Symp. on Environmental Degradation of Materials in Nuclear Power Systems – Water Reactor, NACE, p. 451, 1983.

13. Jacobs, A. J., G. P. Wozadlo, K. Nakata, T. Yoshida, and I. Masaoka, "Radiation Effects on the Stress Corrosion and Other Selected Properties of Type-304 and Type-316 Stainless Steels," Proc. Third Intl. Symp. on Environmental Degradation of Materials in Nuclear Power Systems – Water Reactor, The Metallurgical Society, Warrendale, PA, pp. 673–681, 1987.

14. Chung, H. M., R. V. Strain, and R. W. Clark, "Slow–Strain–Rate–Tensile Test of Model Austenitic Stainless Steels Irradiated in the Halden Reactor," in Environmentally Assisted Cracking in Light Water Reactors Semiannual Report July 2000 – December 2000, NUREG/CR–4667, Vol. 31, ANL–01/09, pp. 22–32, 2002.

15. Chung, H. M., R. V. Strain, and R. W. Clark, "Slow-Strain-Rate-Tensile Test of Model Austenitic Stainless Steels Irradiated in the Halden Reactor," in Environmentally Assisted Cracking in Light Water Reactors Semiannual Report January – December 2001, NUREG/CR–4667, Vol. 32, ANL–02/33, pp. 19–28, 2003.

16. Andresen, P. L., and F. P. Ford, "Irradiation Assisted Stress Corrosion Cracking: From Modeling and Prediction of Laboratory & In–Core Response to Component Life Prediction," Corrosion/95, Paper No. 419, NACE, Houston TX, 1995.

17. Jenssen, A., and L. G. Ljungberg, "Irradiation Assisted Stress Corrosion Cracking of Stainless Alloys in BWR Normal Water Chemistry and Hydrogen Water Chemistry," Proc. Sixth Intl. Symp. on Environmental Degradation of Materials in Nuclear Power Systems – Water Reactor, R. E. Gold and E. P. Simonen, eds., Minerals, Metals & Materials Society, pp. 547–553, 1993.

18. Jenssen, A., and L. G. Ljungberg, "Irradiation Assisted Stress Corrosion Cracking. Post Irradiation CERT Tests of Stainless Steels in a BWR Test Loop," Proc. Seventh Intl. Symp. on Environmental Degradation of Materials in Nuclear Power Systems – Water Reactor, G. Airey et al., eds., NACE, pp. 1043–1052, 1995.

19. Chopra, O. K., E. E. Gruber, and W. J. Shack, "Fracture Toughness and Crack Growth Rates of Irradiated Austenitic Stainless Steels," NUREG/CR–6826, ANL–03/22, 2003.

20. Chopra, O. K., E. E. Gruber, and W. J. Shack, "Crack Growth Behavior of Irradiated Austenitic Stainless Steels in High-Purity Water at 289°C," Proc. Eleventh Intl. Symp. on Environmental Degradation of Materials in Nuclear Power Systems – Water Reactor, American Nuclear Society, pp. 1027–1035, 2003.

21. Hazelton, W. S., and W. H. Koo, "Technical Report on Material Selection and Processing Guidelines for BWR Coolant Pressure Boundary Piping, Final Report," NUREG–0313, Rev. 2, 1988.

22. *ASM Handbook*, ASM International, Vol. 6, p 202, 1993.

23. *Welding Handbook Seventh Edition Volume 2*, "Welding Processes-Arc and Gas Welding and Cutting, Brazing, and Soldering," American Welding Society, Chapter 6, 1978.

24. Angeliu, T. M., P. L. Andresen, E. Hall, J. A. Sutliff, and S. Sitzman, "Strain and Microstructure Characterization of Austenitic Stainless Steel Weld HAZs," Corrosion/2000, Paper 00186, NACE, 2000.

25. Angeliu, T. M., P. L. Andresen, J. A. Sutliff, and R. M. Horn, "Intergranular Stress Corrosion Cracking of Unsensitized Stainless Steels in BWR Environments," Proc. Ninth Intl. Symp. on Environmental Degradation of Materials in Nuclear Power Systems – Water Reactor, AIME, pp. 311–318, 1999.

26. Andresen, P. L., T. M. Angeliu, W. R. Catlin, L. M. Young, and R. M. Horn, "Effect of Deformation on SCC of Unsensitized Stainless Steel," Corrosion/2000, Paper 00203, NACE, 2000.

27. Andresen, P. L., T. M. Angeliu, L. M. Young, W. R. Catlin, and R. M. Horn, "Mechanism and Kinetics of SCC in Stainless Steels," Proc. Tenth Intl. Symp. on Environmental Degradation of Materials in Nuclear Power Systems – Water Reactor, NACE, 2001.

28. Odette, G. R., and G. E. Lucas, "The Effects of Intermediate Temperature Irradiation on the Mechanical Behavior of 300–Series Austenitic Stainless Steels," J. Nucl. Mater. 179–181, 572–576, 1991.

29. James, L. A., and D. P. Jones, "Fatigue Crack Growth Correlation for Austenitic Stainless Steels in Air," Proc. Conf. on Predictive Capabilities in Environmentally–Assisted Cracking, PVP Vol. 99, R. Rungta, ed., American Society of Mechanical Engineers, New York, pp. 363–414, 1985.

30. Shack, W. J., and T. F. Kassner, "Review of Environmental Effects on Fatigue Crack Growth of Austenitic Stainless Steels," NUREG/CR–6176, ANL–94/1, May 1994.

31. Alexandreanu, B., and G. S. Was, "A Priori Determination of the Sampling Size for Grain Boundary Character Distribution and Grain Boundary Degradation Analysis," Phil. Mag. A 81 (8), 1951–1965, 2001.

32. Andresen, P. L., "Similarity of Cold Work and Radiation Hardening in Enhancing Yield Strength and SCC Growth of Stainless Steel in Hot Water," Corrosion/02, Paper 02509, NACE, 2002.

NRC FORM 335
(2–89)
NRCM 1102,
3201, 3202

U. S. NUCLEAR REGULATORY COMMISSION

BIBLIOGRAPHIC DATA SHEET

(See instructions on the reverse)

1. REPORT NUMBER
(Assigned by NRC. Add Vol., Supp., Rev., and Addendum Numbers, if any.)

NUREG/CR–
ANL–04/20

2. TITLE AND SUBTITLE

Crack Growth Rates of Irradiated Austenitic Stainless Steel Weld Heat Affected Zone in BWR Environments

3. DATE REPORT PUBLISHED

MONTH	YEAR
February	2005

4. FIN OR GRANT NUMBER

Y6388

5. AUTHOR(S)

O. K. Chopra, B. Alexandreanu, E. E. Gruber, R. S. Daum, and W. J. Shack

6. TYPE OF REPORT

Technical

7. PERIOD COVERED (Inclusive Dates)

8. PERFORMING ORGANIZATION – NAME AND ADDRESS (If NRC, provide Division, Office or Region, U.S. Nuclear Regulatory Commission, and mailing address; if contractor, provide name and mailing address.)

Argonne National Laboratory
9700 South Cass Avenue
Argonne, IL 60439

9. SPONSORING ORGANIZATION – NAME AND ADDRESS *(If NRC, type "Same as above": if contractor, provide NRC Division, Office or Region, U.S. Nuclear Regulatory Commission, and mailing address.)*

Division of Engineering Technology
Office of Nuclear Regulatory Research
U.S. Nuclear Regulatory Commission
Washington, DC 20555–0001

10. SUPPLEMENTARY NOTES

William H. Cullen, Jr., NRC Project Manager

11. ABSTRACT (200 words or less)

Austenitic stainless steels (SSs) are used extensively as structural alloys in the internal components of reactor pressure vessels because of their superior fracture toughness. However, exposure to high levels of neutron irradiation for extended periods can exacerbate the corrosion fatigue and stress corrosion cracking of these steels by affecting the material microchemistry, material microstructure, and water chemistry. Experimental data are presented on crack growth rates of the heat affected zone (HAZ) in Types 304L and 304 SS weld specimens before and after they were irradiated to a fluence of 5.0×10^{20} n/cm^2 (E > 1 MeV) (≈0.75 dpa) at ≈288°C. Crack growth tests were conducted under cycling loading and long–hold–time trapezoidal loading in simulated boiling water reactor environments on Type 304L SS HAZ of the H5 weld from the Grand Gulf reactor core shroud and on Type 304 SS HAZ of a laboratory–prepared weld. The effects of material composition, irradiation, and water chemistry on growth rates are discussed.

12. KEY WORDS/DESCRIPTORS *(List words or phrases that will assist researchers in locating this report.)*

Crack Growth Rate
Neutron Irradiation
Heat Affected Zone
BWR Environment
Dissolved Oxygen
Austenitic Stainless Steels

13. AVAILABILITY STATEMENT

Unlimited

14. SECURITY CLASSIFICATION

(This Page)

Unclassified

(This Report)

Unclassified

15. NUMBER OF PAGES

16.ICE PR

NRC FORM 335 (2–89)